

Masterarbeit

Screening for physical and biological determinants of bacterial swarm development

vorgelegt von
Sven Brieden
Matrikelnummer: 3137970

Fachbereich Physik
Philipps-Universität Marburg

07.02.2020
Erster Gutachter: Prof. Dr. Knut Drescher
Zweiter Gutachter: Prof. Dr. Victor Sourjik

Contents

1	Introduction	1
1.1	Zusammenfassung	1
1.2	Abstract	2
2	Theoretical background	3
2.1	Bacterial swarming	3
2.2	Dark field illumination	6
2.3	Heating and thermometer	6
3	Material and Methods	9
3.1	High throughput library generation	9
3.1.1	Total DNA isolation protocol	11
3.1.2	Transformation protocol	12
3.2	Development of a Screening Robot	12
3.2.1	Proof of concept with test installation	12
3.2.2	Design requirements	14
3.2.3	Imaging	14
3.2.3.1	Lightsources	16
3.2.3.2	Optical setup	17
3.2.3.3	List of components	20
3.2.4	Heating Circuit	23
3.2.4.1	List of components	23
3.2.5	Robot actuators	26
3.2.5.1	List of components	26
3.2.5.2	Multiplexing sample holder	26
3.2.5.3	List of components	27
3.2.6	Electronic circuit design	27
3.2.7	Hardware control and software	30
3.2.7.1	Heating control	30
3.2.7.2	Software-technical substructures	31
3.2.7.3	Graphical User Interface	31

4 Performance and Limitations of the Screening Robot	33
4.1 Performance of the imaging system	33
4.1.1 Light sources	33
4.1.2 Theoretical image resolution	33
4.1.3 Practical image resolution	35
4.1.4 Optical distortion	35
4.2 Actuators: precision and performance	37
4.2.1 Positioning performance	37
4.2.2 Theoretical resolution	37
4.2.3 Speed	38
5 Optimization swarming protocol	39
6 Conclusions	41

CHAPTER 1

Introduction

1.1 Zusammenfassung

Bakterien zeigen in der Natur unterschiedliche Möglichkeiten der aktiven Ausbreitung, welches als kollektives Verhalten interpretiert werden kann und dem Schwärmen von Vögeln oder Fischen ähnelt. Die vorliegende Arbeit befasst sich mit der Beobachtung von bakteriellem Schwärmen auf Oberflächen. Diese stellt auf Größenskalen von μm relativ zur Größe der Organismen eine schnelle Bewegung von aktiven Zellen in einer Monolage dar. Eine weitere Bewegungsform besteht mit dem bakterielle Schwimmen in planktonischer Umgebung, wobei die Zellen ebenfalls durch rotierende Flagellen angetrieben werden. Beiden Bewegungsformen unterscheiden sich im Falle des hier untersuchten *Bacillus subtilis* durch verschiedenartige Zellkörper, einer erhöhten Anzahl von Flagellen und unterschiedlichen Genexpression. Die Bewegung von Bakterien auf Oberflächen ist weniger verstanden als ihre Schwimmbewegung in Flüssigkeiten [1, 2, 3].

Bisherige Studien sind auf die Analyse einzelner mikroskopischer Blickfelder beschränkt. Diese erweitert Hannah Jeckel [4] durch die mikroskopische Verfolgung der sich ausbreitenden Bakterien. An diese Forschungsergebnisse wird angeknüpft und ein rein makroskopischer Ansatz entwickelt. Das Verhalten einzelner Zellen ist damit nicht mehr auflösbar, folglich aber deren kollektive Bewegung.

Der technische Aspekt dieser Arbeit ist auf das sogenannte High-Throughput-Screening (HTS) gelegt, welches von der Wirkstoffentwicklung übernommen wurde. Es ermöglicht, eine Vielzahl von Experimente in kurzer Zeit teilweise parallel durchzuführen [5]. Durch das Screenen einer sogenannten Knockout Library (Sammlung von Bakterien, bei denen jeweils ein Gen vollständig abgeschaltet ist), erhoffen wir ein vertieftes Verständnis über den genetischen Einfluss auf das bakterielle Schwärmen.

Ziel dieses Projektes ist es, einen Roboter zum automatischen Durchführen von Screens, etwa für bakterielle Schwärme oder Biofilme, zu entwickeln.

1.2 Abstract

In nature, bacteria show several different possibilities for the active spreading. This spreading can be interpreted as collective behavior, resembling swarming of birds or fish. The present work reports on the observation of bacterial swarms on surfaces, a rapid movement of active cells in a monolayer. In this medium, each cell is driven by rotating flagella, similar to bacterial swimming in liquid environments. These two forms of movement are distinguished by the different types of cell bodies, the number of flagella and a varying gene expression. The movement of bacteria on surfaces is less understood than their swimming behavior in liquids [1, 2, 3].

Previous studies have been limited by the scope of view of microscopes. The work by Hannah Jeckel's extended the field of vision by macroscopic tracking of the spreading bacteria. These results are pursued, and a purely macroscopic approach is developed. As a result, the behavior of individual cells is no longer visible, but their collective movement becomes apparent [4].

The application of High-Throughput Screening (HTS) is increasingly used in microbiology adapted from drug development. HTS enables carrying out a high throughput, partially in parallel in a short time [5]. By screening a collection of bacteria, each has one gene, which is made completely inoperative (knockout gene library). We are aiming to gain a deeper understanding of the genetic components of bacterial swarming. The aim of this project is to develop a robot for automatically performing screens, for example for bacterial swarms or biofilms.

CHAPTER 2

Theoretical background

This chapter aims to give a short theoretical introduction to the concepts used in the design and building a robot for automated screening of bacterial swarming. This section clarifies the scientific process and the resulting work from a biological, physical and robotic perspective.

2.1 Bacterial swarming

In the following, the aspect of bacterial swarming is described, required for the biological background of this work. As this behaviour is a key to understand the objective of this work, further subjects in order to clarify the *Bacillus subtilis* Library are presented.

The word Bacteria comes from the old Greek word for rod, which is a type of biological single-cell organism, classified under the Prokaryota domain. The average size of most bacteria is between 0.2 and 2.0 micrometre. Many bacteria can not only move in a targeted manner, they can also communicate with other species. Their behaviour of movement and communication can be explained as a collective multicellular phenomena. Many bacteria can move with mechanisms like swimming, swarming, gliding, twitching, sliding, and darting. Swarming is the fastest type of movement with a Colony expansion rates of up to 10 $\mu\text{m}/\text{s}$ [6]. It is a way to colonize surfaces for different reasons like availability of nutrients. [Figure 2.1 Bacterial motility](#) visualizes two mechanisms and their power like the rotating flagella. The focus of this work is on Bacterial swarming as a rapid multicellular movement across a surface.

In previous work from Patrick JE, an inhibited swarming motility is shown for the many commonly used laboratory strains [7]. Swarming is promoted by high growth rates and requires generally an energy-rich and solid medium [7, 8]. To observe it in the laboratory agar, concentrations from 0.3% up to 1.0% are required, depending bacteria. During the preparation of the agar the drying time, the temperature and the associated water content must be planned having an important influence in healthy swarming and preventing swimming happens, resulting in a comparable colony[9]

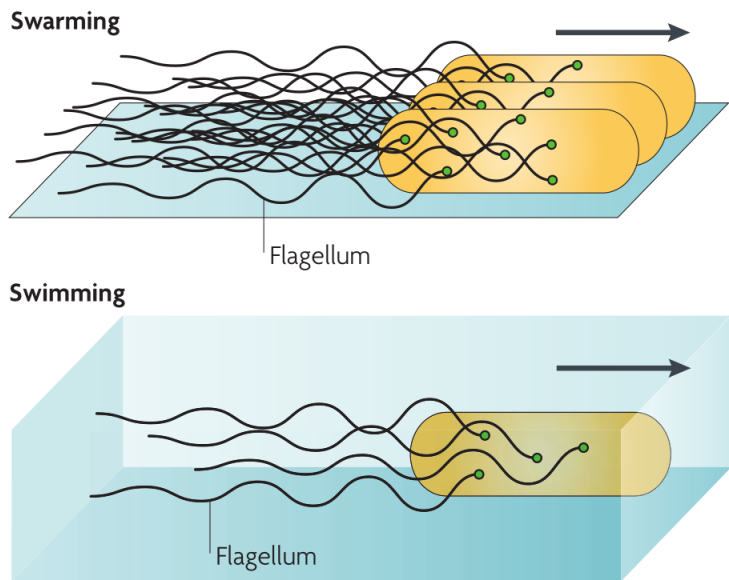


Figure 2.1: Different modes of motility for bacteria are shown. Many cells are not motile if then under specific circumstances affected by environmental factors. The different types of movements are be subdivided into v categorise: movement in a liquid and on a surface. The remaining are movements across a surface. The rotating helical flagella are the motor for the swarming mechanism, which we are focusing in.[1, p.635]

Bacteria requires flagella, cell-cell interactions and the presence of a surfactant for swarming. The flagella are helical filaments that rotate like screws [10]. They can be made visible with fluorescence microscopy or electron microscopy. In literature it is also shown, that bacterial mutants with defects in flagella loose the ability of swarming motility [11].

An example of different patterns while swarming is shown in the [Figure 2.2 Swarming colonies](#). The behavior of (e) *Salmonella typhimurium* and in the present work considered the *B. subtilis* wild types show a similar pattern. Dendrites, strongly pronounced by (b) *Pseudomonas aeruginosa*, were also observed to some extent in wild-type *B. subtilis*.

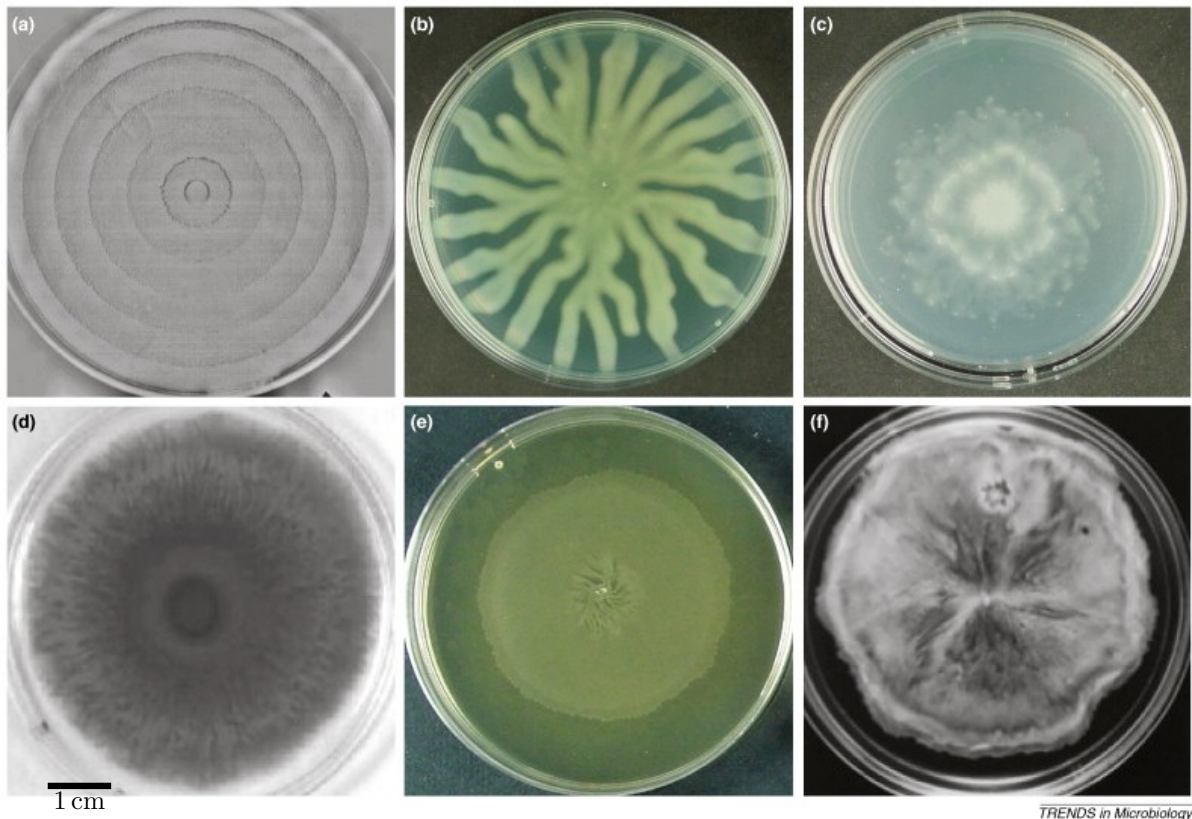


Figure 2.2: Swarming colonies of different bacteria on agar plates. The morphology suspects various observable features besides the growing rate. The shown bacteria are:
(a) *Proteus mirabilis*, (b) *Pseudomonas aeruginosa*, (c) *Rhizobium etli*,
(d) *Serratia marcescens*, (e) *Salmonella typhimurium* and (f) *Escherichia coli*. Adapted from [12].

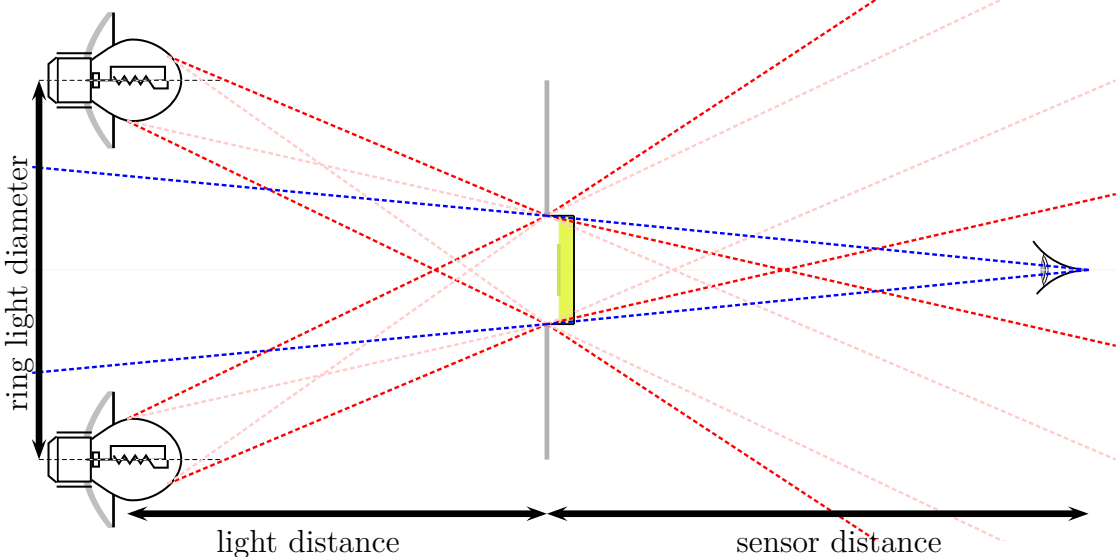


Figure 2.3: Schematic representation of the optics with the beam paths (dashed lines). A Petri dish with bacteria is illustrated in the middle. The gray line around the Petri dish represents the plate holder for positioning, blocking out the light around the dishes.

2.2 Dark field illumination

Much of the work in this project contributes to an engineering procedure. Beneath the conception for the experimental approach, many decisions focussing on design decisions are made.

Imaging has been very important in the history of biology. The greatest progress has been made with tools such as the microscope. Also in this work, the optical presence is the most weighty information about the bacteria. In the field of electronics, the work relies on the theory of heat development in electrical resistors.

There are two main types of lighting. For this work, the dark field illumination is more important than the brightfield illumination. This technique is mainly used to highlight surface defects, scratches or engravings. Small, even unstained, objects can be observed with high contrast. Darkfield lights are usually built in the form of flat ring lights, which must be attached close to the test object. In contrast to brightfield illuminations, the light that is reflected from the surface of the test object is aimed at positions outside the field of view of the camera. [Figure 2.3 Schematic Dark Field Illumination](#) shows the structure and the light paths in such an arrangement. Large ring lights, spotlights and line lights can be used as darkfield lighting. [13]

2.3 Heating and thermometer

Electric heating elements are the most common form of build in heating mechanisms. These components are built-up by a heating coil and covered to the exterior by an isolating material. The heating can be explained simplified by converting the electrical current to heat on electrical resistance. The performance of which is calculated from the voltage U and the internal fixed resistance R : $P = \frac{U^2}{R}$. For further power regulations, the circuit

of the individual heating coils can be varied at a given voltage. This changes the overall resistance. It is calculated in case of a series connection of N resistance changes by the sum of the individual respective components R_{0i} :

$$R_{\text{total}} = \sum_{n=1}^N R_n = R_1 + R_2 + \dots + R_N \quad (2.1)$$

This results with a parallel connection using N resistors:

$$R_{\text{total}} = \frac{1}{\sum_{n=1}^N \frac{1}{R_n}} \quad (2.2)$$

The overall resistances R_{total} is calculated by the following expression

$$R_{\text{ges}} = \frac{R}{N} \quad (2.3)$$

CHAPTER 3

Material and Methods

3.1 High throughput library generation

Our goal is to prepare a screen of a *B. subtilis* mutant library for swarm behavior and biofilm formation. Gene circuits and regulators at tempo-spatial dynamic resolution are aimed to be analyzed. To achieve this goal, a single deletion mutant library in NCIB3610 background is needed, which is well studied *B. subtilis* strain for Swarm and biofilm behavior. Single deletion mutant library of *B. subtilis* exists in 168(1A1) background[14], which neither makes well structured colony biofilm nor shows swarming because of mutations in genes needed for swarming and biofilm formation.

The work was divided into two parts. First, the DNA was extracted for the complete collection, and in part two, the transformation of the DNA into competence cells was carried out. The following chapters show the microbiological protocols.

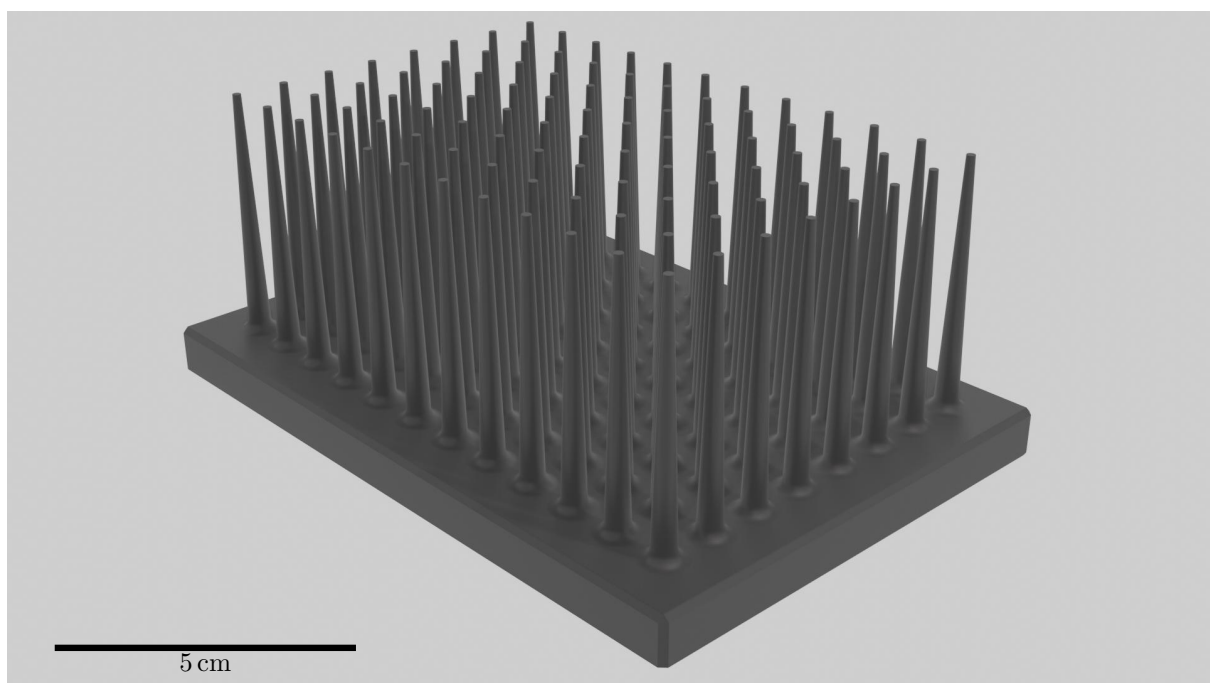


Figure 3.1: The Microplate Replicator for Microtiter plates with 96 wells is used to perform inoculating from dens LB-Medium or to spot individual colonies on Agar. It is built by the MPI Precision Engineer Horst Henseling. The pin length was required for the inoculation in the deep well strip tubes at step 2.1 in the [Total DNA isolation protocol](#).

3.1.1 Total DNA isolation protocol

- Day 1 1.1 Prepare a strip tube box to autoclave.
- Day 2 2.1 Grow culture in strip tubes (96 well plate set up) in 500 μ l LB + Kan7.5 with shaking (190-220 rpm) for 20 hr. Covering the plate with a parafilm.
- Day 3 3.1 Prepare the mix of lysozyme in TE buffer:
2 ml Lysozyme (100 mg/ml stock) + 5 ml TE (10xTE stock)/plate.
3.2 Incubate with lysozyme mix (70 μ l/well) at 37°C with shaking at 180 rpm for 30 min.
3.3 Make 6 ml (10% SDS)+400 μ l Prtk (20 μ g/ml) mix per plate.
3.4 Add 64 μ l of above mix per well and incubate at 60°C for 20 min in a water bath.
3.5 Add 450 μ l of Ph:Chl ready to use mix (Roth). Close the tubes with strip caps. Mix the tubes and centrifuge the whole plate of tubes in the bigger rotor for 15 min with 1.5K rpm. Clean the centrifuge afterward to avoid any phenol residue.
3.6 Transfer 450 μ l upper layer in an Eppendorf tube (1.5 ml). Use a multi pipette, and by a carefull transferring, avoid any debris.
3.7 Add 90 μ l NaOAC (3M) + 450 μ l Isopropanol in each tube and mix it by vertexing.
3.8 Incubate at -20°C in the freezer overnight.
- Day 4 4.1 Centrifuge tubes with 14 K rpm for 15 min.
4.2 Throw the supernatant (850 μ l) with the help of a multi pipette. Use the lowest power to aspirate the liquid by not touching the pellet.
4.3 Add 600 μ l of 70% Ethanol in tubes. Keep them at RT for 10 min for washing.
4.4 Throw supernatant (600 μ l) again with a multi pipette. Take the rest of the residue carfully out with a normal pipette carefully.
4.5 Dry the pellet in 37°C incubator for 10 min. Check some tubes if there is no ethanol.
4.6 Add 50 μ l of 60 °C preheated ddH₂O in each tube and leave at RT for 30 min to dissolve the DNA.
4.7 Check some of the DNA quality by nanodrop.
4.8 Store the DNA at -20°C with proper labeling of the stock number.
4.9 Randomly select some tubes and take Sul DNA. Incubate with RNase for 30 min and run a gel to see the quality of DNA.

3.1.2 Transformation protocol

- Day 1 1.1 Grow kdb26 (or any other *B. subtilis* strain to be used as background) in MC medium overnight at 37 °C in Shaking incubators.
- Day 2 2.1 Dilute 1/50 in competent medium.
2.2 Inoculate 40 µl of diluted cells in each well of 96 well plate.
2.3 Mix 4 µl of total DNA from above isolation in individual wells.
2.4 Incubate the plate at 37 °C incubator without shaking for 16-18h. To maintain the humidity, keep water in a tray inside the incubator. Close the plates tightly with parafilm.
- Day 3 3.1 Add 10µl LB containing 15 µg/ml Kan (final concentration 3 µl/ml in each tube) for the enrichment of transformants. Incubate the plate at 37 °C for another 6 h.
3.2 Inoculate 5-10 µl of the total mix on Kan7.5 LB agar plate. Best use 96 well plate, where individual wells are filled with LB agar+Kan. Incubate the plate at 37 °C for 20-24h.
- Day 4 4.1 Inoculate individual transformants on another plate containing Spec100. Incubate the plate for another 24 h.
- Day 5 5.1 Make a culture of transformants in Kan7.5+Spec100 by inoculating individual colonies and grow overnight.
- Day 6 6.1 Stock by adding glycerol. Use robots to add the glycerol

3.2 Development of a Screening Robot

The following chapter describes the creation of a robot and explains the design decisions. It is essential to mention that both accuracy and a high-throughput are necessary. When screening genomic variance, one speaks not of 10 or 100 variations, but of a few thousand. The built robot should be able to perform this task and is optimized for the swarming behaviour observed in the Knockout library of *B. subtilis* but can easily adapted to other macroscopic screening tasks, for example biofilm formation. This chapter contains the design decisions and describes the robot and its components. The following chapter then reports on its performance.

3.2.1 Proof of concept with test installation

Before this project started, it was necessary to test its feasibility. For this purpose, the unmodified *B. subtilis* wild type was chosen and observed while swarming on a standard agar LB plate. Hannah Jeckel also analyzed this behaviour during her work under a microscope. In previous work was checked whether macroscopic detection was possible[4].

The optical structure consists, bottom-up, of a ring light (outside the field of view of the camera), a glass pane with a template for positioning the Petri dishes, and an

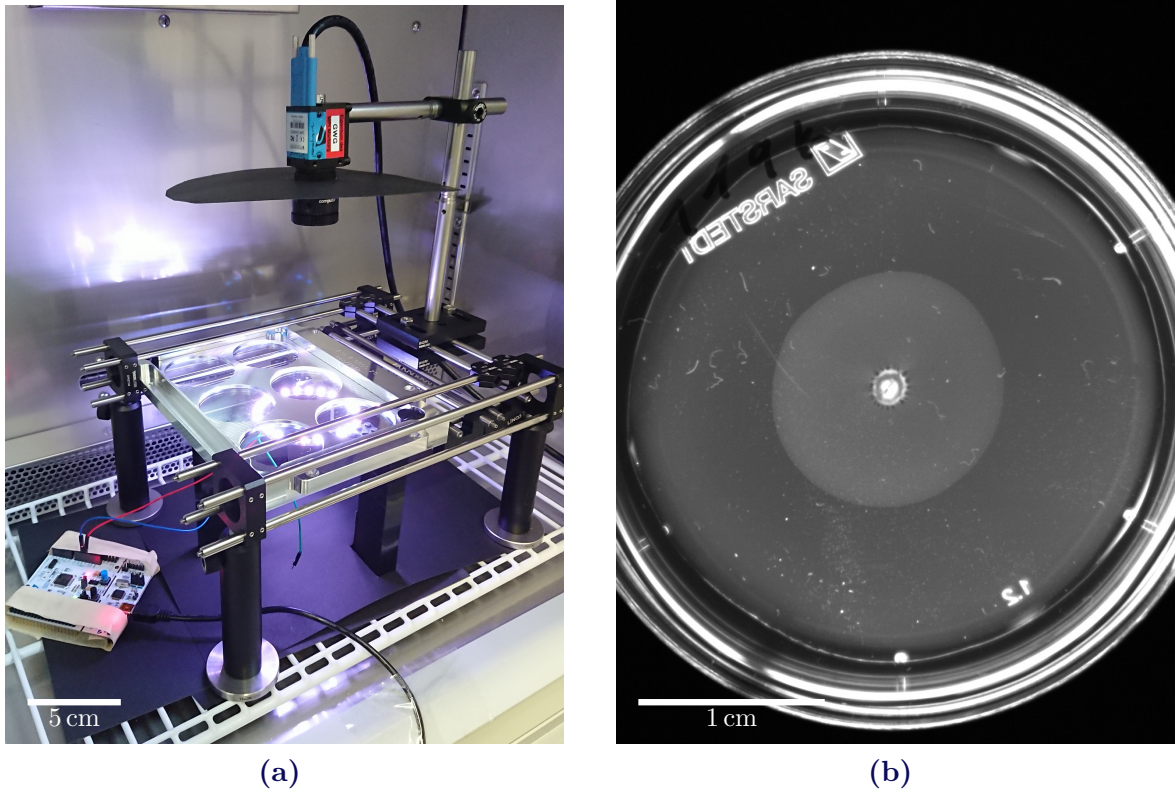


Figure 3.2: The "proof of concept" model with the basic components: Lighsource, plate holder for one Petri dish and a camera. It was located in an incubator to control the environmental temperature. The first pictures and time series with the static camera have confirmed the feasibility.
 a) View of the first test setup located in an incubator.
 b) A swarming *B. subtilis* in a small Petri dish after 2 hours.

inverted Petri dish with the bacterial culture on agar. The recording is taken by the setup-included camera.

Figure 3.2 Proof of concept model shows the static demonstrator model, which was used to produce the first data. For test purposes, this setup was placed in an incubator. The initial setup had no motor functionalities, therefore just a single Petri dish was observed. This method was well suited to optimize the optics and its parameters.

The first tests were illuminated with a converted desk lamp and the results can be seen in **Figure 3.2b First swarming *B. subtilis***. This demonstrated the applicability of the used approach and the swarming behaviour can be recognized. The results were promising in the sense that some properties such as growth rate, morphology and symmetry can be determined. It also turned out that the inoculating step, with its parameters (amount of bacteria and its position), has a significant impact on the quality and reproducibility of the results. The analysis has to be based on equivalent start conditions, so the initial amount of the bacteria must also be consistent. The exact positioning of the inoculate simplifies the subsequent analysis of the data and increases the amount of information since a larger area can be covered before the bacteria reach a border.

3.2.2 Design requirements

The core competencies and specifications for the robot to screen biological processes are listed:

- **Plate holder:**

- Number of samples with fixed positions ≥ 48
- Round cell-culture dish, radial growth expected
- Samples from each other biologically separated
- Little mechanical forces (wiggling) to the samples
- Illumination: transmitted from the bottom
- Other forms of adaptive use (such as 96-well plate, larger plates)

- **Light source:**

- Low-temperature radiation
- Darkfield and Brightfield exposure
- High homogeneity of intensity
- Small construction size

- **Camera:**

- Field of view \geq samples size
- Recording rate ≥ 0.5 FPS
- Controllable via Matlab and μ Manager
- Fluorescence

- **High-throughput mechanics:**

- Time between the repetition of the same sample: ≤ 5 minutes
- \Rightarrow Speed $\geq 1\text{m}/\text{min}$
- Load: 1kg with horizontal movement
- Position precision $\leq \pm 1$ mm
- Ambient temperature ≤ 40 °C
- Working hours $\geq 5\text{h} / \text{day}$ for 4 months
- Controllable via Matlab

- **Heating:**

- Temperature equal over all samples
- Temperature accuracy $\leq \pm 0,5$ °C
- Temperature range ≤ 40 °C
- Warm-up time ≤ 30 min

3.2.3 Imaging

Light has a significant impact on machine vision systems. Aiming high contrast in a dark field technique, stray light inside the robot has to be avoided.

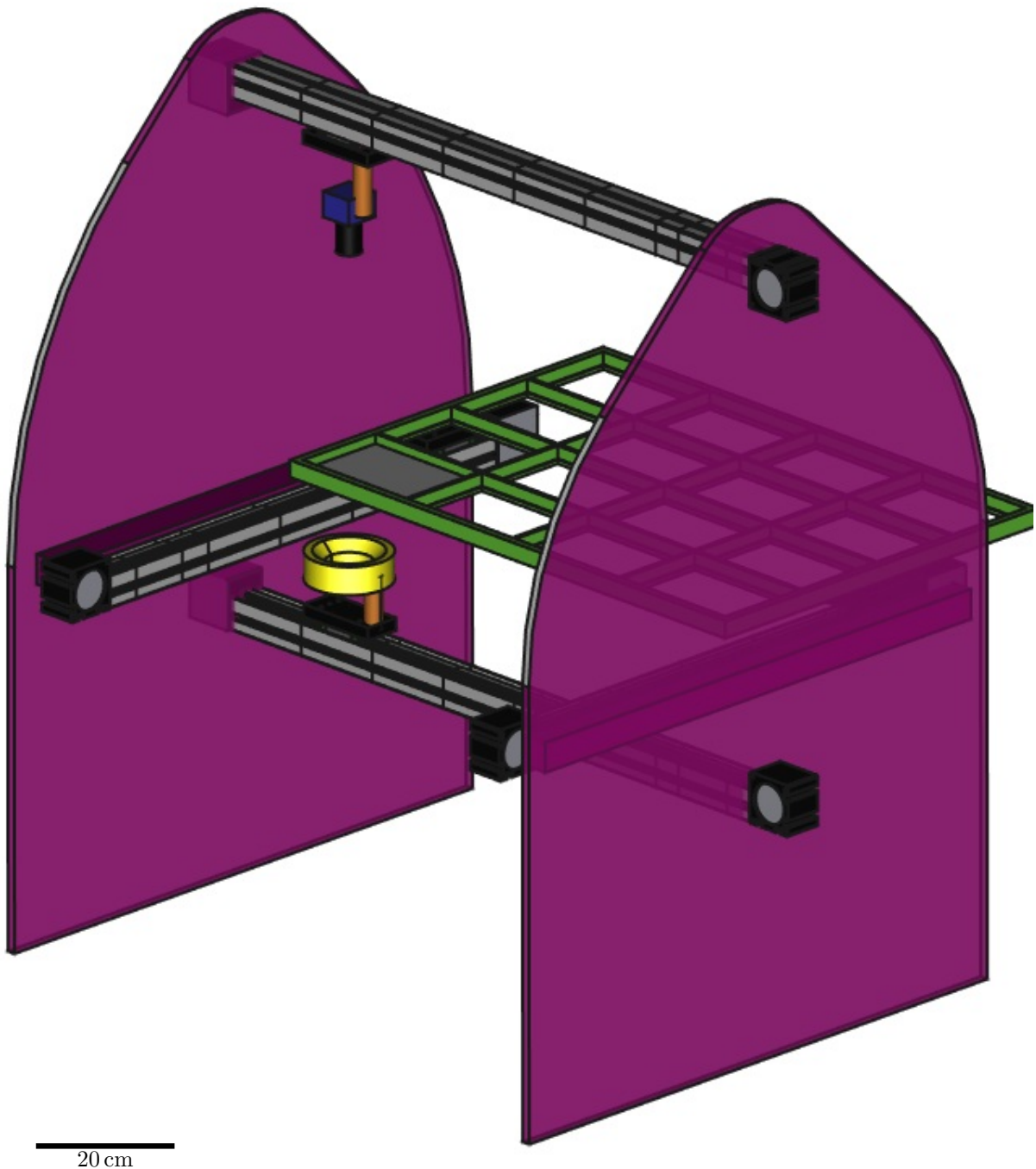


Figure 3.3: The first design had a camera over the plate holder and the light source underneath, as was the case in the proof of concept. Besides, the plate holder can be moved automatically in the vertical (X) direction and the camera and light source in the forward (Y) direction. Color coding: sample holder green, light source yellow, camera blue, motorized linear units gray, support structure purple

3.2.3.1 Lightsources

An important part of this project is the choice of light source. As part of the optics, it affects the quality of the result in a way that cannot be easily corrected later on. Here, the initial design decision is chosen on the optical principle of dark field illumination, where the unscattered beam from the light source is excluded from the image. This technique, the exact opposite of a bright field illumination, is typically applied to an upright microscope. Only the scattered light passes to the image and gives a dark background around the object. The result is showing an improvement of the contrast of an unstained sample and makes transparent specimens visible. [13, p. 28.28]

The mono layer is transparent but may be seen when incident light is reflected off the surface or when oblique light is transmitted through the agar. [1, p. 638]

This quote about visibility of Bacterial swarming shows the difficulty in this endeavour, and the need for dark field illumination in this project to increase the contrast. A circular lamp must be used according to this optical principle to ensure a symmetrical illumination. Ring lights (flashes) have been used traditionally for macro photography to ensure shadow-free and soft lighting. The use of large ring lights for portrait photography is in today's approaches. The latest application of ring lights can be seen in headlight systems in the automotive sector. This illumination specification is chosen in the project by its stability and simplicity.

In contrast to conventional SMD LEDs, chip-on-board LEDs (so-called COBs) consist of a multi chip arrangement in which many individual low-power LED chips are connected in series and parallel. COB LEDs have an emission surface, singular towards the outside, ensuring a homogeneous intensity distribution without optical hotspots. This results in the advantage of a simplified optical design, which can be realized. The design enabled an homogeneous illumination in a circular shape with a minimal form of a few millimetres in height. Figure 3.4 Ring lights homogeneity quantitatively shows the difference of a circular light ring with conventional SMD LEDs (a) and a circular light made with the COB method (b). The Projection on a sheet of paper shows the cone of light at different distances, with both lamps having the same diameter of 90 mm. With its 90 LEDs in a single chip, the COB LED lamp provides a much higher degree of homogeneity than the LED ring with 24 individual LEDs.

Three lamps were compared in the test installation for a qualitative statement regarding the resulting image quality. They are listed in Table 3.1 List of the tested ring lights. The different technologies processes have emphasized the contrast to different extents.. Furthermore it was possible to optimize the distance between the circular light sources and the sample (see subsection 3.2.1 Proof of concept with test installation).

Strong reflections from the light source on the agar in the outer area of the Petri dish are inevitable (see. Figure 3.5 *B. subtilis* after 4h). This is due to the slight curvature of the surface of the agar.

By choosing the concept of dark view with a translucent light source, it was now a matter of determining the light source and finding the working distance. This result mainly requires a high contrast between locations with bacteria and without bacteria. One problem is that there is only a rotational symmetry. Here, contrast in the middle of

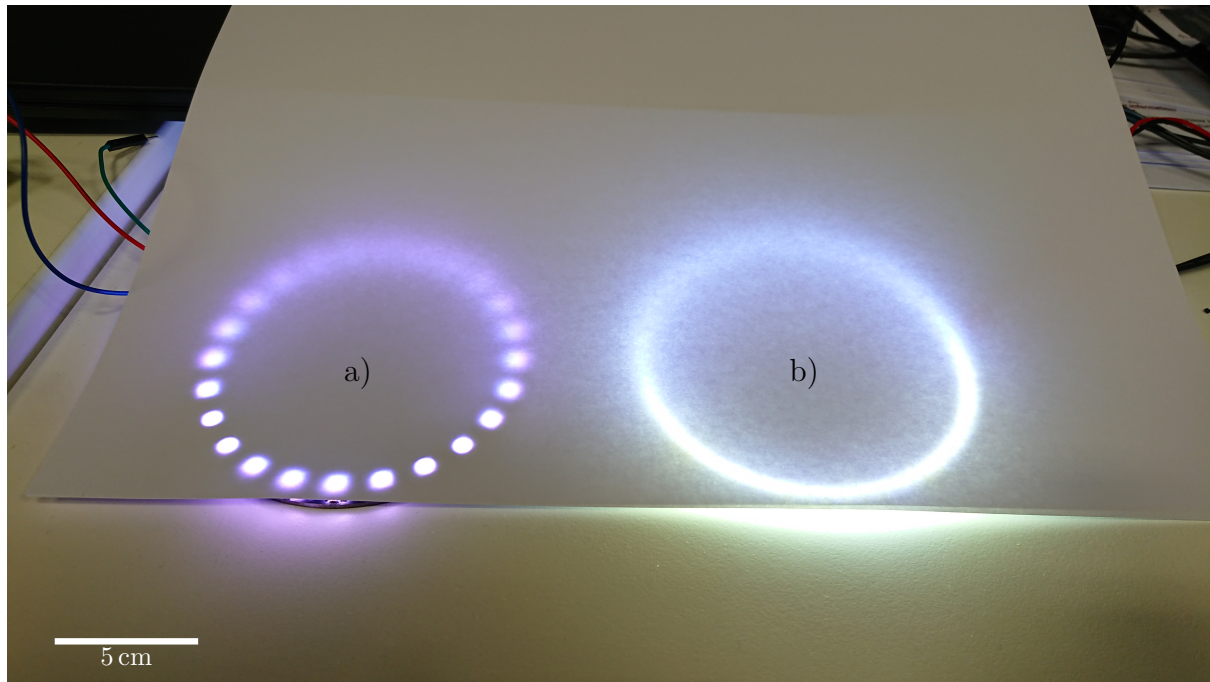


Figure 3.4: Ring lights made with the COB method tested to increase radial homogeneity of single LEDs ring. Ring b) is showing a higher homogeneity and intensity in comparison to a).

the petri dish and at the edges has to be ensured. The following experiment was carried out in order to empirically determine the optimal light source and geometry. An agar plate was inoculated at various positions. The positions were previously marked symmetrically on the Petri dish backside (see [Figure 3.6a Multipoint inoculated Petri dishes](#)). For evaluation, the differences in brightness were calculated with ImageJ. 15 swarm were analysed with the mean over four points for each swarm (see [Figure 3.6b Multi Swarming analysis](#)). The large LED ring generates the highest contrast. An additional advantage of the large LED ring and its larger distance from the sample is that possible positioning errors contribute with a smaller angle uncertainty. Further experiments are carried out with the large LED ring.

3.2.3.2 Optical setup

In this chapter, the optical setup is described after the light source and distance have been fixed. A [Six-Position Motorized Filter Wheel](#) is integrated for later fluorescence

Diameter [mm]	Number of LEDs	E. Power [W]	Technology
90	24	2	individual LEDs
120	120	4	COB (Chips on Board)
160	186	5	COB (Chips on Board)

Table 3.1: List of the tested ring lights. The different technologies processes have emphasized the contrast to different extents.

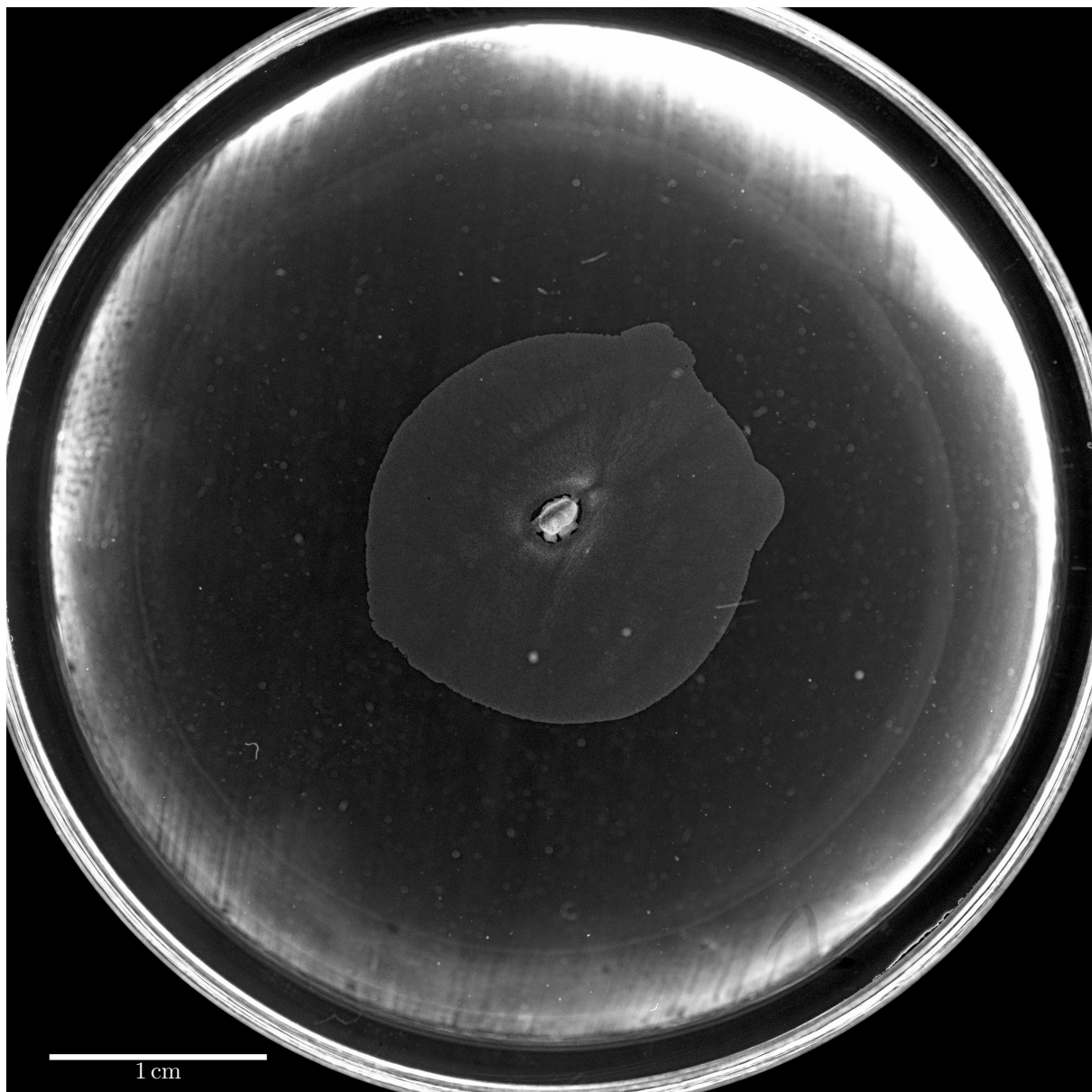


Figure 3.5: *B. subtilis* while swarming in a 3.5 cm Petri dish after 4 hours at 37°C. It was inoculated in the center and grew symmetrically to the outside. Reflections from the light source can be seen at the edge of the Petri dish. This design creates enough contrast for the later automated analysis.

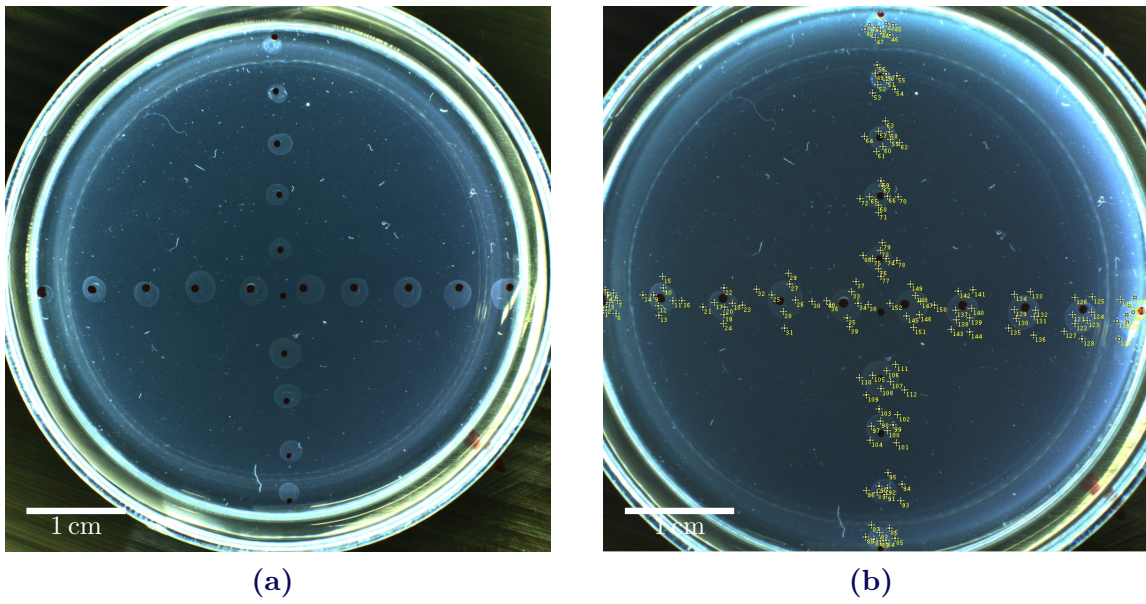


Figure 3.6: Method and results of the lighting test.

- a) Test sample: Petri dish with several *B. subtilis* swarms, inoculated at the previously marked points (black dots). After three hours they had grown large enough to test with different optical settings.
- b) Evaluation: to determine the contrast (swarm vs. no-swarm), images pixels were analysed with ImageJ. The yellow elements are the positions for this analysis.

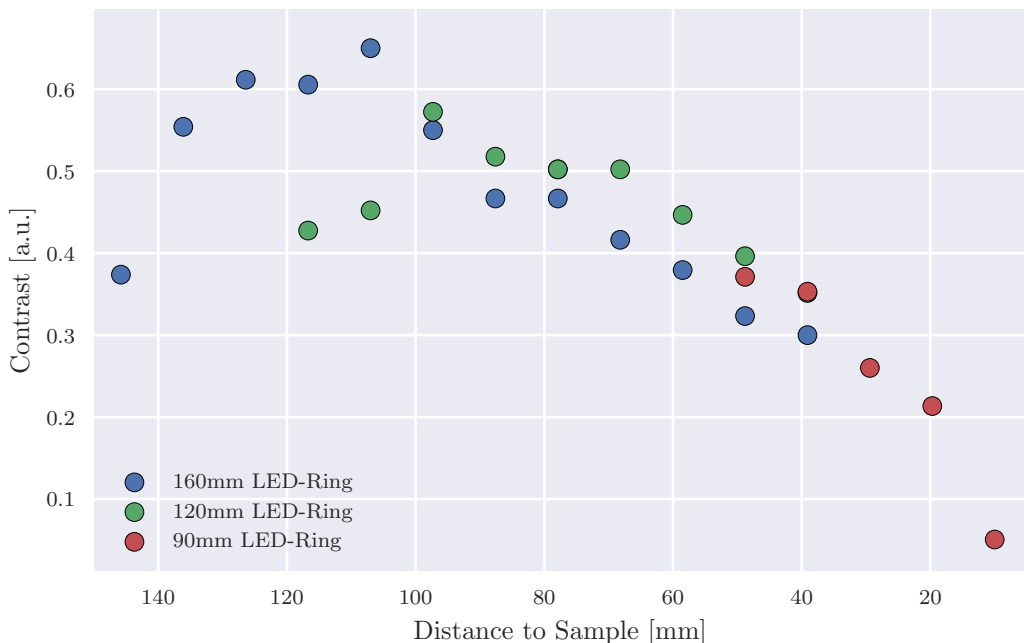
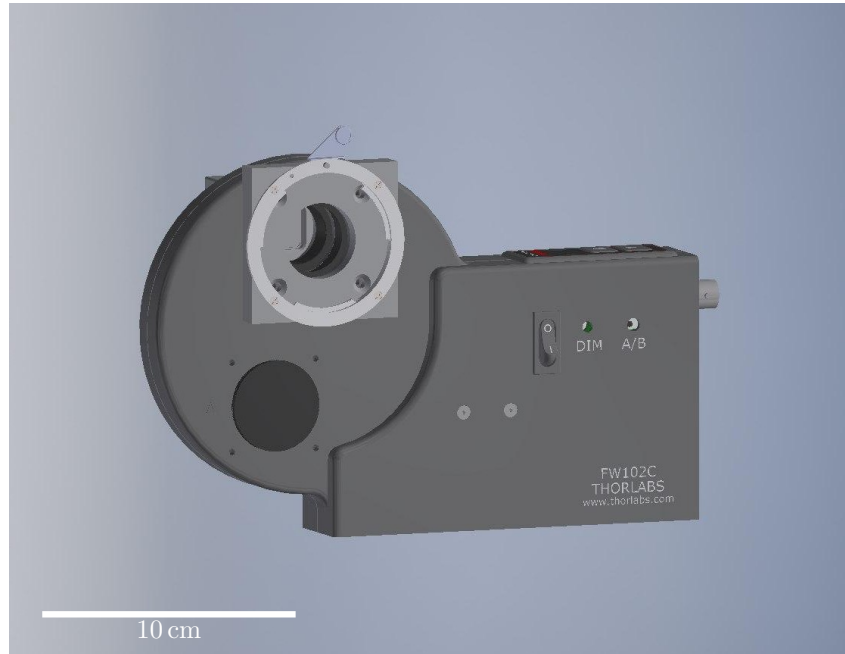


Figure 3.7: Result: Representation of the contrasts of different light sources over the distance between light source and sample. In this case, the higher contrast results in a better image quality. The main difficulty lies in creating good contrast over the entire surface. Therefore, swarm fronts were generated and analyzed at 20 positions.

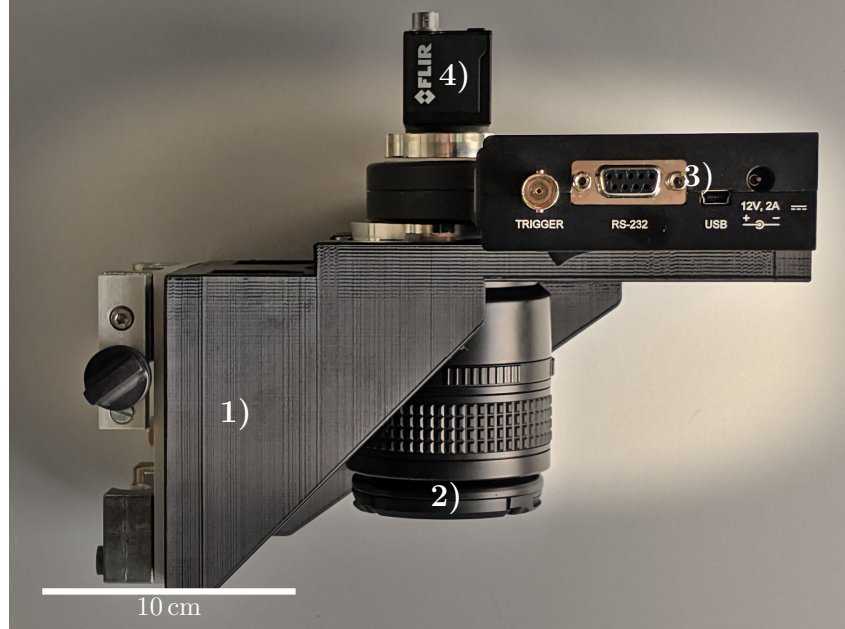
experiments. The filter wheel has a relatively small opening and small filters compared to filter mounts on objectives. As a result, they cannot be attached in front of a lens. It was necessary to build a camera construction in house with enough space between the lens and the camera chip. Two different standards were combined, each with different flange focal distance (distance between the end of the lens and the image plane). [Figure 3.8 Optical setup](#) shows the diagram and a photo of the manufacturing construction. A large load-bearing element(1) was 3D-printed. It connects the adjustable robot adaptation with the filter wheel. The camera and lens are attached to the filter wheel. [Figure 3.9 Vibrio cholera microscopic](#) shows the imaging capacity of the camera system at the maximum magnification. In addition to experiments with swarming bacteria, the robot is also used for all kinds of macroscopic images.

3.2.3.3 List of components

Component	Product Name (Link)	Manufactury	Quantity
Power Supply 12V	LS 10810 Unterputz Netzteil	LUPUS-Electronics	1
LED Ring Lamp	160mm HALO COB LED Rings	Hoping	2
USB Camera	BFS-U3-200S6M-C	FLIR	1
Macro Lens	60mm f2.8 AF Nikkor Micro D	Nikon	1
Filter Wheel	FW102C	Thorlabs	1



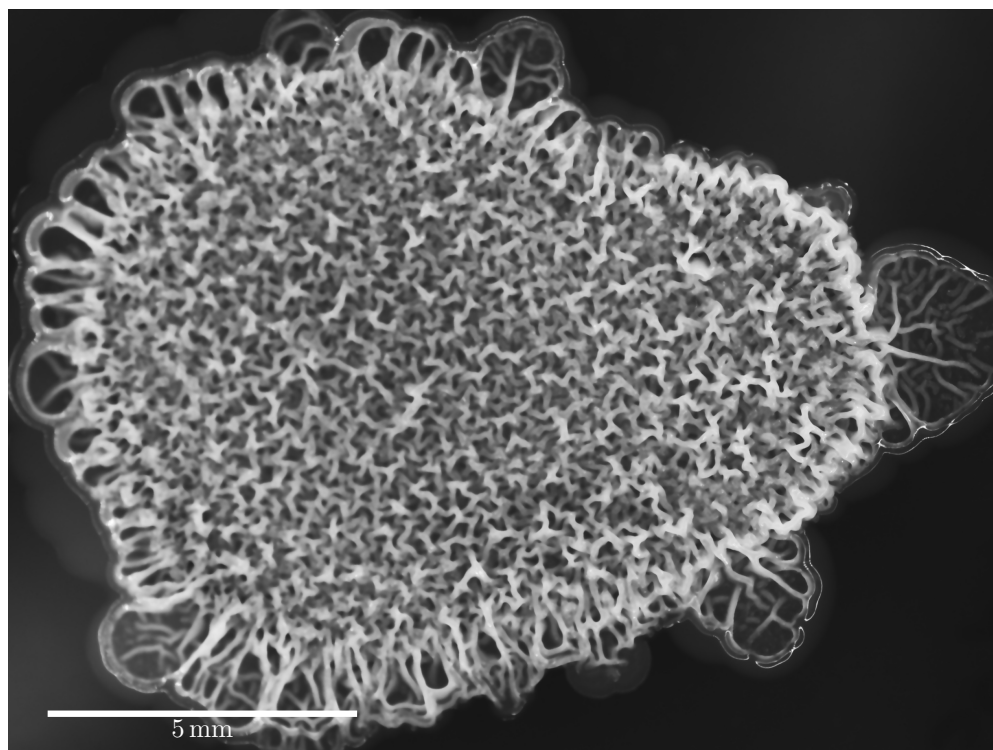
(a)



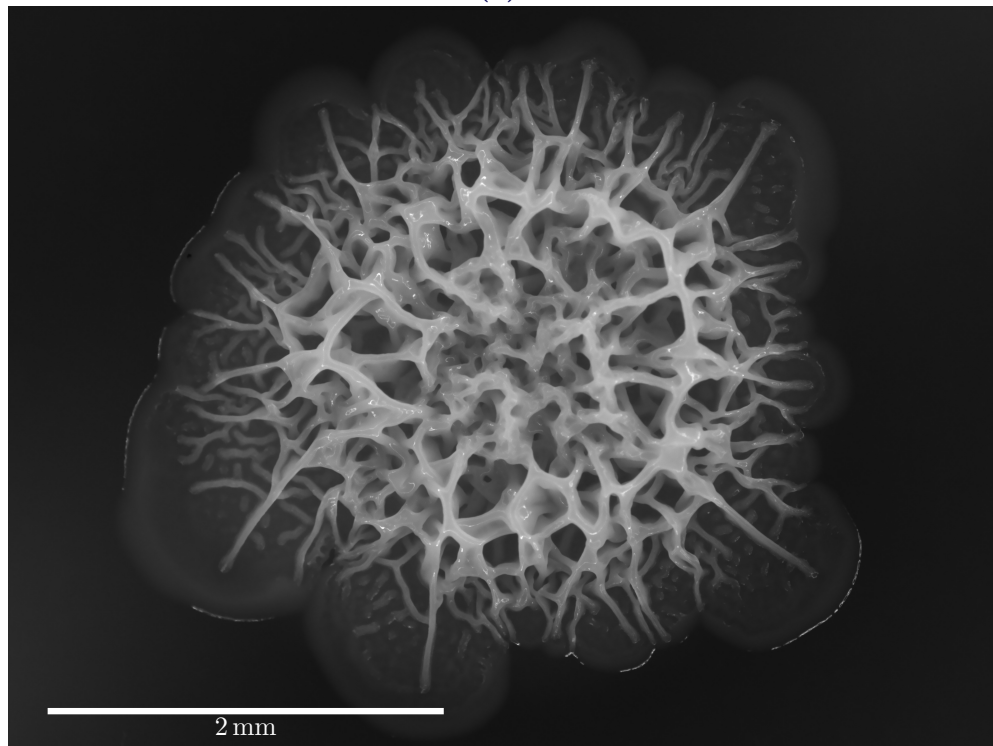
(b)

Figure 3.8: The optical setup is shown. The construction consisting of an f-mount lens with an f-mount adapter screwed onto a filter wheel and a c-mount camera adapted. The official flange focal distance is preserved, which means that the optical performance of the lens is not affected. Macro capability is ensured thanks to a 1:1 magnification.

- a) The rendered illustration shows the motorized filter wheel and with the self build F-Mount connector.
- b) Final construction with: 1) Camera-Robot-Mount, 2) Macro-Lens, 3) Filter Wheel and 4) Camera.



(a)



(b)

Figure 3.9: A rugose strain from *Vibrio cholerae* was prepared to assess the performance of the optical system. Due to the high pixel density, it is possible to take microscopic pictures, fulfilling the macroscopic image requirements.

3.2.4 Heating Circuit

The environmental temperature influences bacterial behaviour on a significant number of regulators [15]. Temperature is an essential and critical factor to realize reproducible swarming development. The following section aims to explain how to create a uniform, smooth and stable ambient temperature.

Various incubator chambers are working with circulating air heating (e.g., [Heidolph Heating Module Incubator 1000](#)). These heating modules have the advantage of easy installation and the disadvantage of incalculable temperature gradients, resulting by uneven airflows. Furthermore, the regulation of the ambient temperature of the bacteria by measuring the air temperature would be indirect and inaccurate.

The homogeneity and stability of the temperature is implemented by indirect heating using thermal radiation by two thick heated metal plates. The whole bottom and the entire hat of the chamber are covered to guarantee the uniform radiation and small temperature gradients.

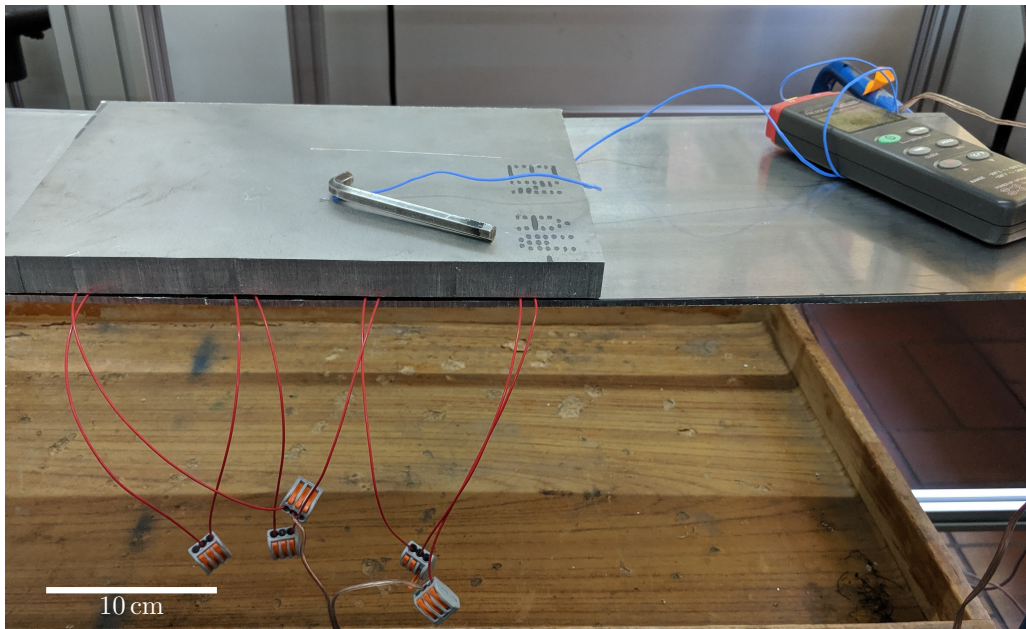
Half of the heating surface also represents the table surface. This part of the robot can be touched intentionally or unintentionally by the user and requires to follow safety procedures. The maximum temperature was based on the DIN EN ISO 13732-1:2008-12[16]: Ergonomics of the thermal environment - Evaluation method for human reactions in contact with surfaces - Part 1: Hot surfaces. There are temperature values at which there is a considerable danger for the user. The maximum surface temperature of metal $t_{\text{surface}} = 67^{\circ}\text{C}$ prevents operators from being injured.

The heating of the robot is realized by silicone heater pads. These consist of a silicone mat with etched foil heating elements for wide temperature ranges. Several pads in electrical series and parallel connection give constructive freedoms to optimize the positioning for thermic homogeneity and power. The power can be varied directly through the type of circuit. A [Heater Pad](#) has a resistance of $R = 3\Omega$ (48W at 12V) and is built for an operational voltage of 12V or less. The test setup represents the final robot specifications on a smaller scale. (See Figure 3.10)

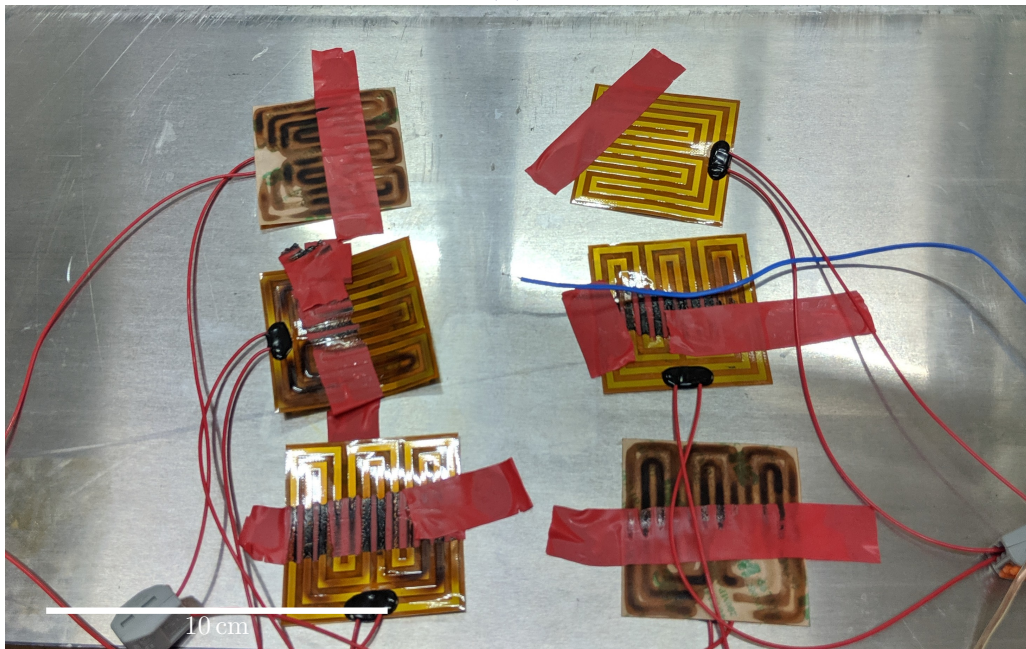
Due to the voltage of the power supply (48V), at least four pads must be in line. The electrical current and thus the power of a line of pads is graduated by adding more pads (ohmic resistances) to the line. A number of 4, 5 and 6 pads in line with the corresponding power of 192W, 153W, and 128W.

3.2.4.1 List of components

Component	Product Name (Link)	Manufactury	#
Heater Pad	Polymide Heizfolie 12V 48W 60mm	Conrad	36
Power Supply 48V	Schaltnetzteil 1.008kW 48V 21A	Mean Well	2
Temperature controller	RS ESM-3721	RS PRO	2
Resistance Thermometer	2-Draht PT1000 Sensor	RS PRO	2
Contactor	Leistungsschütz 22.34.0.230.4620	Finder	2
Bi-Metallic Thermostat	Thermostat Öffner 70°C 15A	Honeywell	6
Inline Fuse Holder	Blade Fuse Holders	Littelfuse	3
Automotive Fuse	Kfz Sicherung blau, 15A	RS PRO	3



(a)



(b)

Figure 3.10: Method and results of the heating test.

- Heating test setup with 1 cm thick metal plate to measure the power distribution.
- The heating output was defined by varying the electric circuits and the positioning of the heat pads.

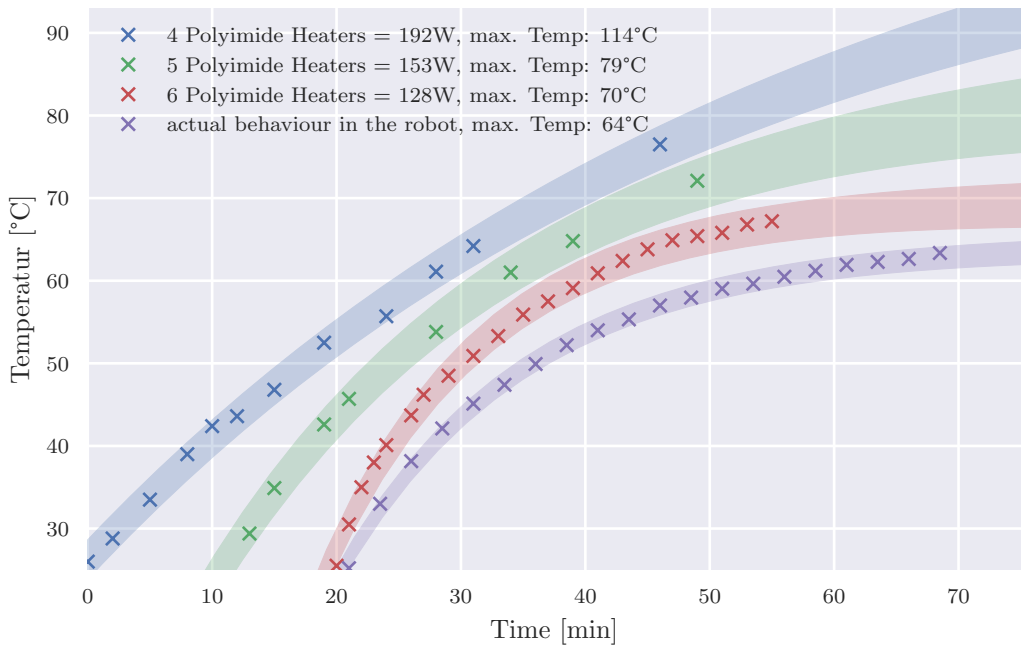


Figure 3.11: Metal surface temperatures in the robot over time with a 95% prediction band. It is mainly determinant by the uncertainty temperature measurement of the respective data points and based on Newton's law of cooling. The maximum temperature, which is given in the legend, was calculated with this prediction band. The experimental setup aims to undershoot a temperature of 67°C, covering the recommended safety guidelines.

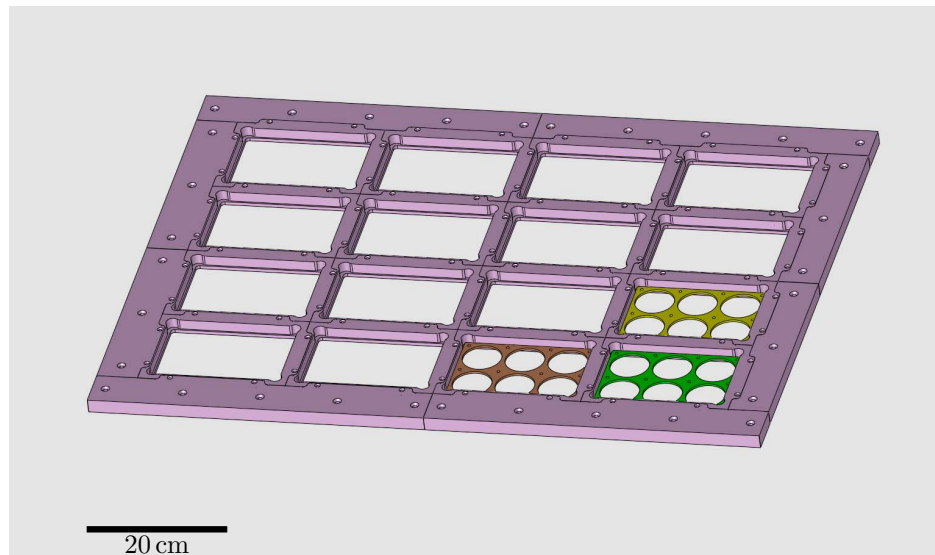


Figure 3.12: Drawing of the plate holder. The templates including holes with a diameter of 55 mm, designed for 96 petri dishes.

3.2.5 Robot actuators

In order to integrate the screening component to the robot, it becomes necessary that the camera and the light move relative to the sample holder. These dimensions are designed to reach an area of 850 mm x 620 mm. Its performance and accuracy is described in section 4.2 Actuators: precision and performance.

3.2.5.1 List of components

Component	Product Name (Link)	Manufactory	no.
Power Supply 5V	POS-35-C, 36 W, 5 V, 7 A	POS	1
Microcontroller	STM32F302R8	STMicroelectronics	2
Motor Driver Board	X-NUCLEO-IHM02A1	STMicroelectronics	2
Inline Fuse Holder	Blade Fuse Holders	Littelfuse	2
Automotive Fuse	Kfz Sicherung braun, 7.5A	RS PRO	3
Axial Fans	4000 Z Series Compact AC	ebm-papst Group	1
Optical Switch	Gabel-Lichtschranke TCST2103	Vishay	4
Cable Chain	E-chain 9, 18.2mm x 19.3mm	Igus	2
Stepper Motor	SM56.2.18.JL1.5	STÖGRA GmbH	4
Linear Axis long	ML 45-11-850 F-Cal-ML-45 LY6914	Maccon GmbH	2
Linear Axis short	ML 45-11-620 F-Cal-ML-45 LY6914	Maccon GmbH	4

3.2.5.2 Multiplexing sample holder

The plate holder was designed with 16 areas on which either six Petri dishes (55 mm), two Petri dishes (92 mm) or two microtiter plates fit. The maximum number is reached by 96 Petri dishes. These are placed on glass panes and centered by templates. (see Figure 3.12 Plate holder). It consists of a reinforced frame of 8 parts and 32 inner struts.

3.2.5.3 List of components

Component	Product Name (Link)	Manufactury	Quantity
Glass panes	Float glass (3x127x185)mm	Schreinerei-Doerr	35
Polystyrene sheets	Druckfeste Steinwolle 20 mm	OBI	5 m ²

3.2.6 Electronic circuit design

The electronics box contains all components for the motor control and temperature control. See [Figure 3.13 Electronics box insight](#) for the technical implementation and [Figure 3.14 Circuit diagram](#) with the circuit diagram. This control unit has a USB connection to the computer and a power supply connection as input. The robot is connected to the electronics box via an eleven connection cable. Each connection cable has up to six individual wires. The following areas are supplied with a cable from the electronics box (see the connectors on the upper area of [Figure 3.14 Circuit diagram](#) right to left):

- heating and thermometer
- power supply for ring light source
- 2x movement unit (camera and light source)
- 2x light barriers
- 2x stepper motor
- reference thermometer

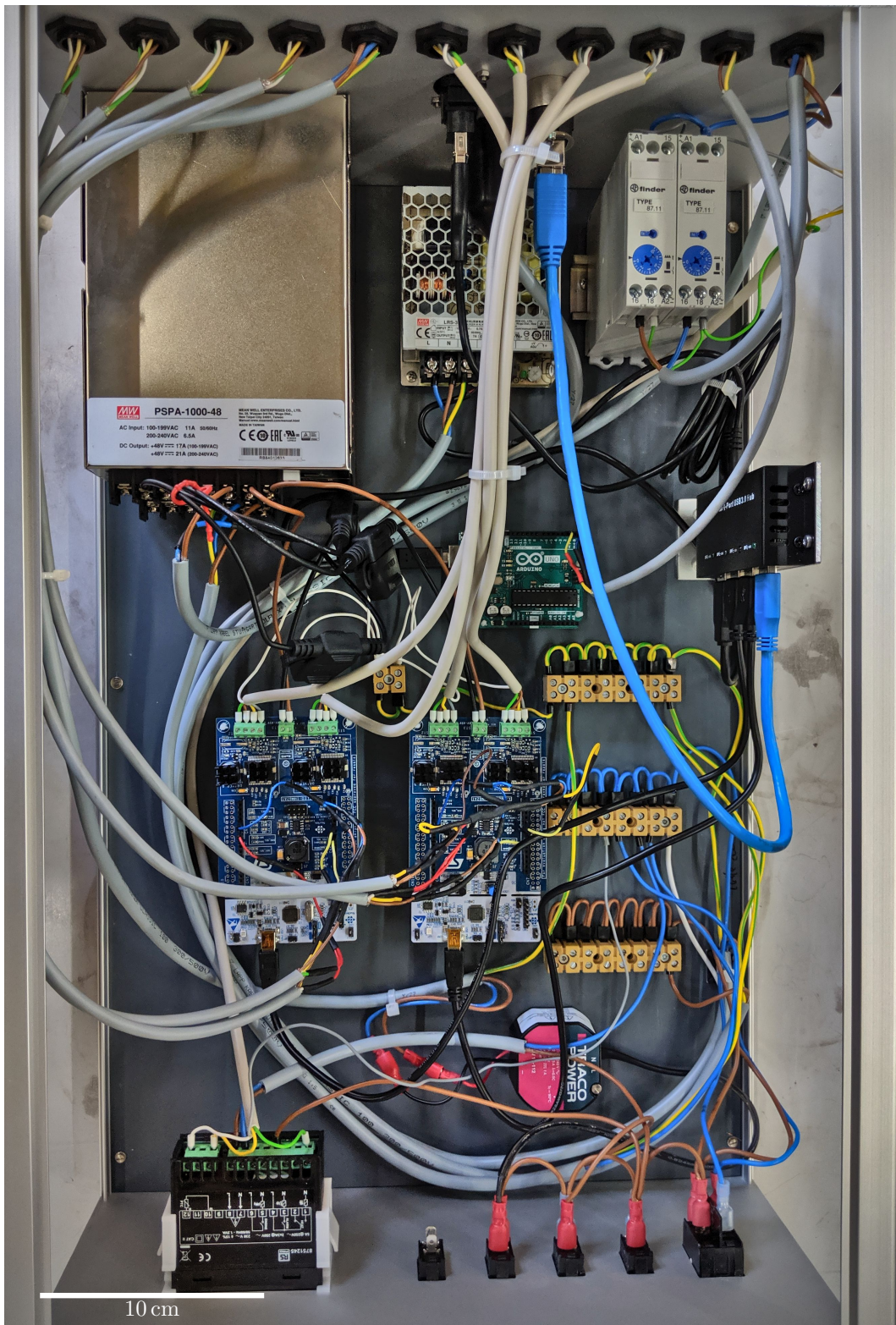


Figure 3.13: The insight of the Electronics box with all the electrical elements from Figure 3.14 Circuit diagram. On the upper area is the back wall with all connections. The lower area houses the supervision for the user. The box is integrated into the housing of the robot.

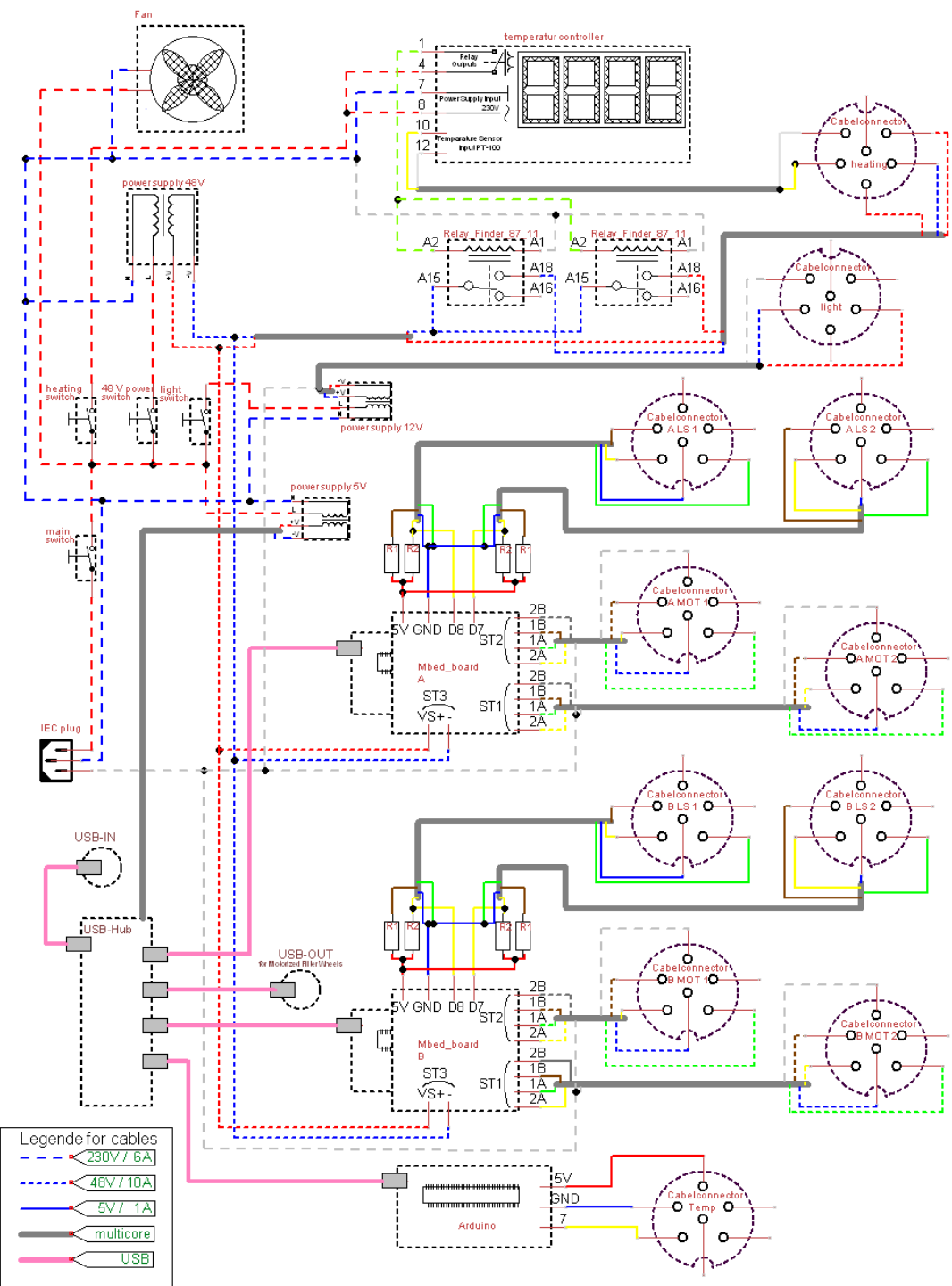


Figure 3.14: Circuit diagram of the electronics box. Different styles of the lines represent different cable types and voltage ranges (see legend).

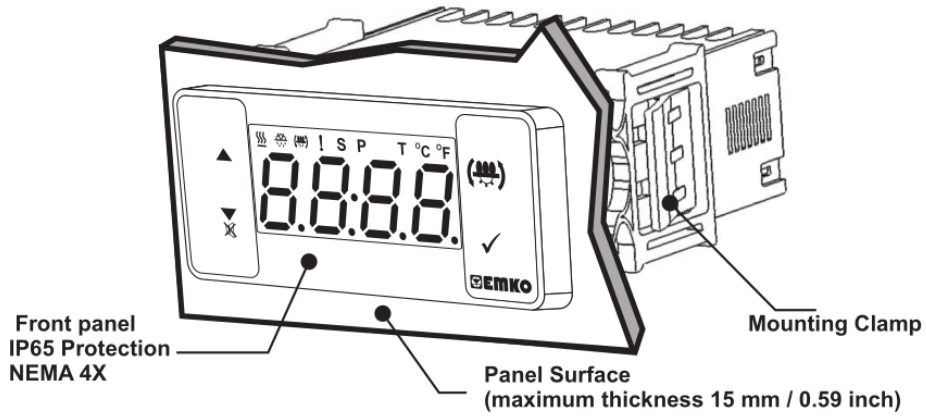


Figure 3.15: The front panel of the temperature controller displays the current measured temperature and the heating status. The desired temperature can be selected using the set button and can be changed using the up and down button. The parameters, as the desired temperature can be adjusted by the manufacturer's buttons. Adapted from [17].

3.2.7 Hardware control and software

This chapter gives an overview of the robot controlling. Many topics from the previous chapters are addressed, which are now viewed from the software side. Most of the components during an experiment, like motors and camera, are managed via a user interface on a computer. The front panel of the robot allows switching on the robot and controlling the heating. The difficulty in the development was the stability of the system, which has to run for several hours without human intervention.

3.2.7.1 Heating control

The temperature is exclusively controlled by two Temperature controller units. The user must set the desired temperature in both units on the front of the robot. One unit heats from underneath, the other from above. The respective units are designed for a complementary performance. The heater should be switched on at least 1 hour before an experiment, with closed doors of the robot, enough to preheat the robot to the desired temperature. The control is optimized for a temperature of 37°C but it can reach any temperature from room temperature up to 50°C. The Resistance Thermometer is placed on the plate holder next to the Petri dishes. The control of the heating power is regulated by a Proportional-Integral-Derivative(PID) controller. The presence of the art control loop mechanism uses feedback to reach a target temperature quickly, without large temperature deviations and without undamped temperature oscillations.

The auto tune function of the Temperature controller units can be used, which determines PID parameters from the temperature gradient during a test run lasting for several hours. For a precise analysis, a thermometer array using wireless sensors ([TFA Dostmann KlimaLogg Pro](#) and [wireless sensor for KlimaLogg Pro](#)) was installed inside the robot. The thermometer readouts were subsequently analyzed. The best results are produced by the following parameters: Temperature controller parameter: P = 1, I = 500, D = 700

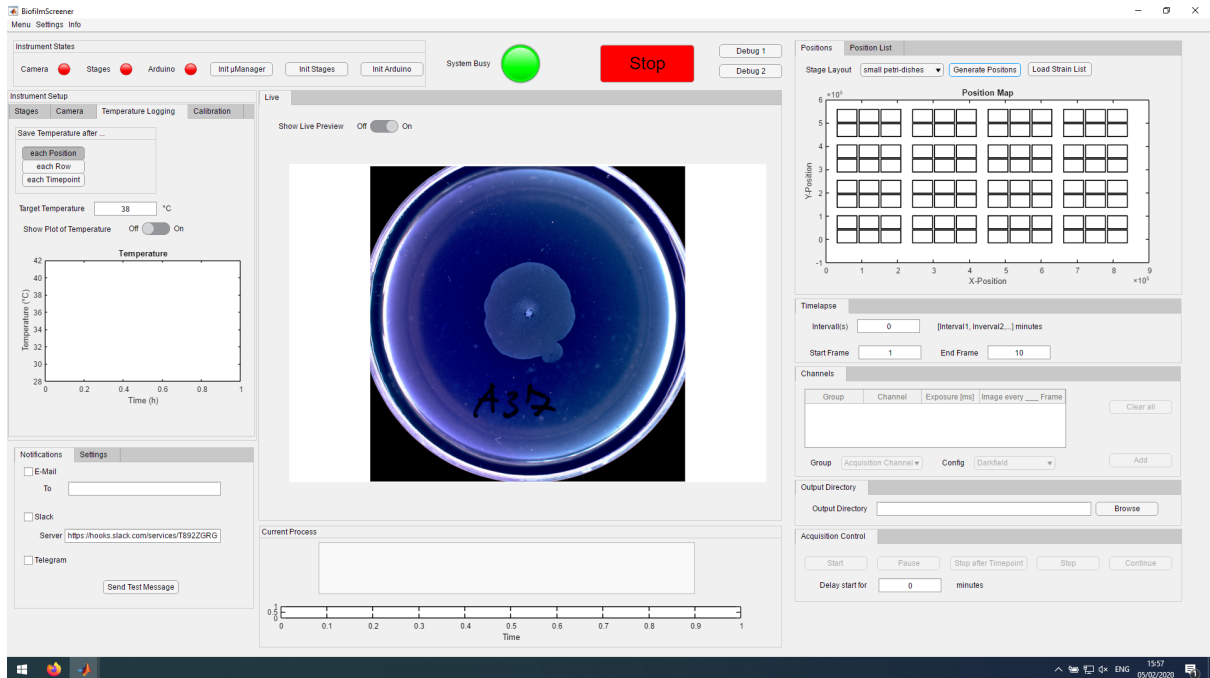


Figure 3.16: The user interface to control the robot is shown. It automatically managed the motors and the camera. A picture preview and a progress bar is built in to give the user feedback on the current status.

3.2.7.2 Software-technical substructures

This section informs about the control of the robot and data collection. For the first iterations, [Python 3.7](#) and [digiCamControl v2.1.2](#) were used for controlling the robot. However, this was replaced by [Matlab r2018b](#) and [micromanager 2.0.0-beta3 20181129](#) for a better integration with the existing software ecosystem. The control of the motors and the read-out of the light barriers states are carried out by two [microcontrollers](#). The communication is ensured by the Matlab software on a computer by comports and a specially adapted Codex. The camera is running by Micromanager, which is controlled via Matlab. In turn, Matlab has a class object for storing the parameters. An object of this class is created when the GUI is started and takes the overall control. Due to the fact that the object functions even without a GUI, a greater flexibility is achieved. [Figure 3.17 Software component diagram](#) shows this software architecture.

3.2.7.3 Graphical User Interface

This section describes the GUI (Graphical User Interface) for controlling the robot. The evaluation of the collected data does not yet have a dedicated GUI. During the programming of the user interface, great value was placed on user-friendliness. Without time-consuming training, the robot should be able to record samples intuitively. Both, single shot and time series are tasks that the user can achieve by this GUI.

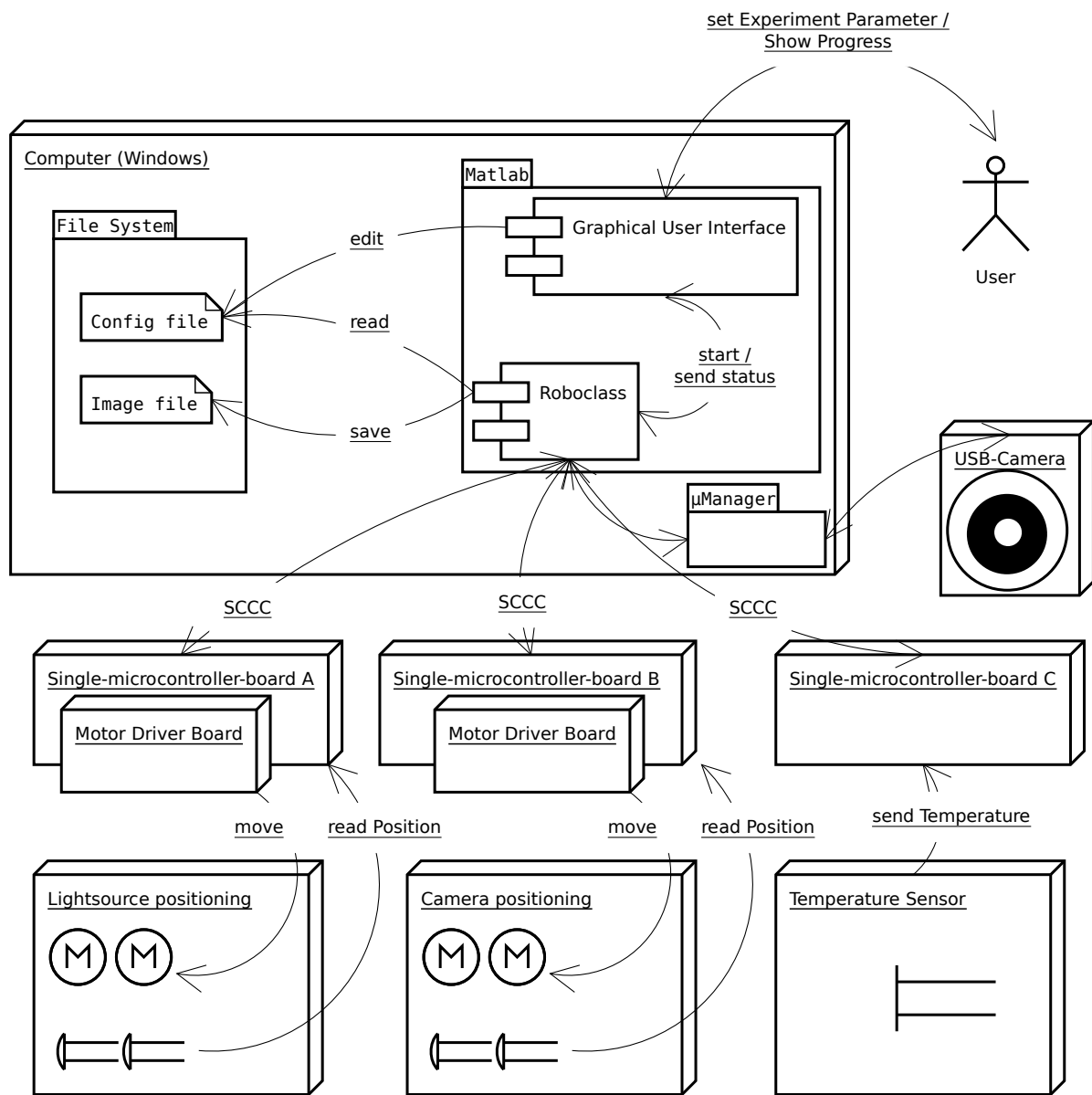


Figure 3.17: Software component diagram illustrating the distribution of the software modules in the system. This organizational chart shows the interaction chains. The core of the control is based in the Roboclass in Matlab on a Computer. The arrows address the connections and the directions.

CHAPTER 4

Performance and Limitations of the Screening Robot

The best observed design for swarming bacteria has two characteristics:

1. Both camera and light source move in two dimensions over all the samples, with the light on the bottom and the camera on the top of the sample.
2. The light source is designed so dark-field exposure is achieved.

These ideas are combined with height adjustment and shown in [Figure 4.1 Final design](#).

4.1 Performance of the imaging system

4.1.1 Light sources

The emission intensity distribution of the LED Ring is shown in [Figure 4.2 Emission distribution](#). It is taken by the Spectrometer SM442 from Spectral Products on average over 50 samples.

4.1.2 Theoretical image resolution

In this subsection, the theoretical resolution of the robot is given within different units. All the results are calculated without any optical aberration.

We start from the Pixel resolution of the image sensors. The [USB-Camera](#) uses a Sony IMX183 sensor with 5472 x 3648 pixel resolution in 3:2 aspect ratio. It supports 20.48M pixel readout at 21.98 frames/s in 12-bit mode. A Unit cell size is 2.4 μm (H) x 2.4 μm (V), according to the diagonal of the sensor of 15.86 mm.[\[18\]](#)

The self-build camera (see [subsubsection 3.2.3.2 Optical setup](#)) with the [Macro lens](#) reaches a magnification of 1:1. The size of the image of an object created by this camera is the object's true size. Therefore the optical resolution is also 5472 x 3648 pixels with a pixel size of 2.4 μm x 2.4 μm .

The resolution can be expressed in line pairs per millimeter (LP/mm), where a line pair has a dark line and an adjacent light line. Theoretically, for each line pair only two pixels

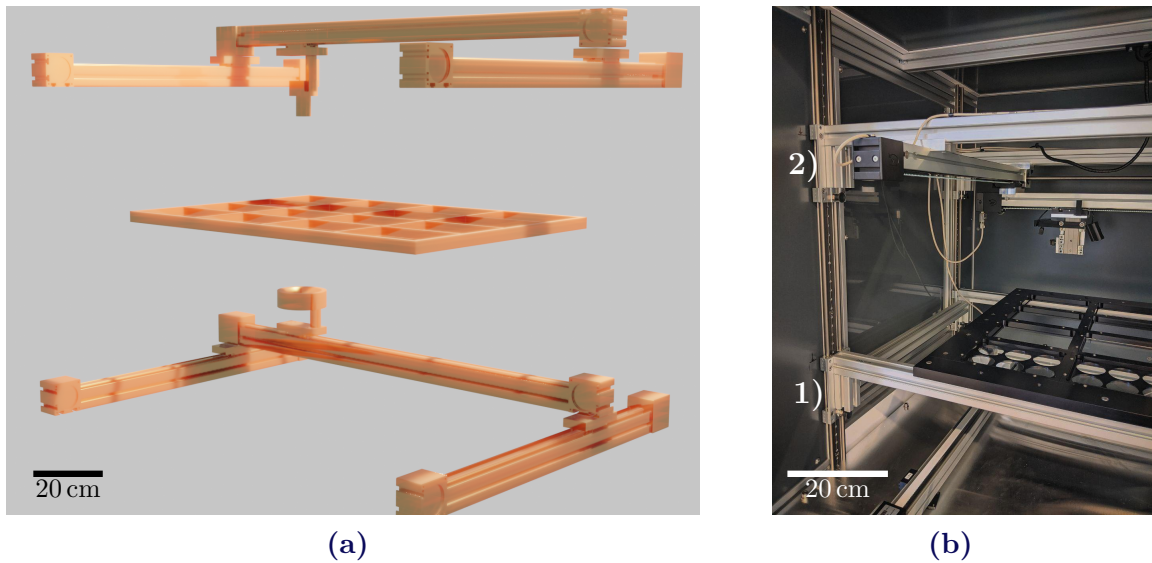


Figure 4.1: Illustration of the constructive interior of the robot.

- a) CAD construction with X-Y movement for the camera (top) and light source (bottom). The plate holder in the middle does not move.
- b) View into the robot showing the height adjustment. The height of the light source is fixed. With 1) the height of the plate holder can be adjusted and the height adjustment for the camera on position 2).

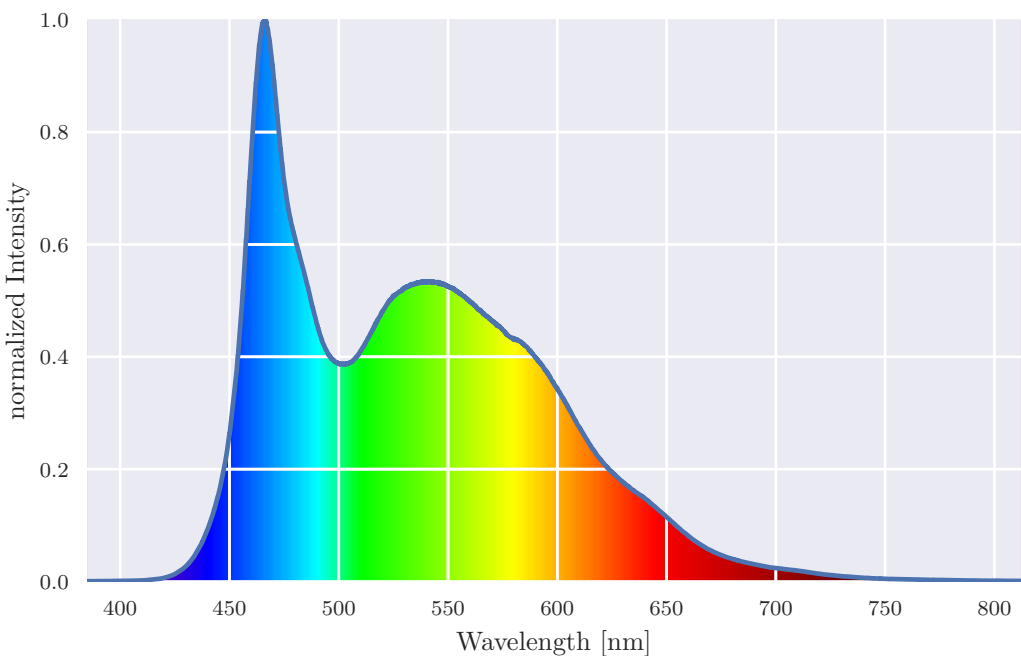


Figure 4.2: Emission intensity distribution of the LED Ring Lamp. Based on measurement by Spectrometer SM442

are needed, in our case $4.8 \mu\text{m}$ per LP. Resulting in the theoretical maximum resolution of: 208.3 LP/mm

4.1.3 Practical image resolution

The resolution of the camera is tested practically, with the help of a test sample. The resolution test target ([R1L1S1P](#)) was placed in the robot instead of the Petri dish. It includes both, a [1951 USAF resolution test chart](#) and Ronchi rulings with [line pairs](#) between 30 lp/mm and 150 lp/mm . The result is shown in [Figure 4.3 Practical image resolution test](#). This picture was taken with the aperture open ($f/2.8$) at the highest magnification. The maximum resolution reaches 150 lp/mm , this corresponds to a pixel size of $3.33 \mu\text{m}$. The theoretical value is 1.39 times better. This resolution is sufficient to take macroscopic pictures of bacterial colonies and swarming bacteria with a few millimetres of width.

4.1.4 Optical distortion

In order to determine the geometric aberrations of optical systems, a millimeter paper was photographed. Hence, the aberration in the outer area to the central area can be calculated. The uncertainty is smaller than a pixel on the sensor and is therefore no longer measurable. This is due to the choice of a 60 mm lens which, in contrast to a wide-angle lens, has a smaller distortion.

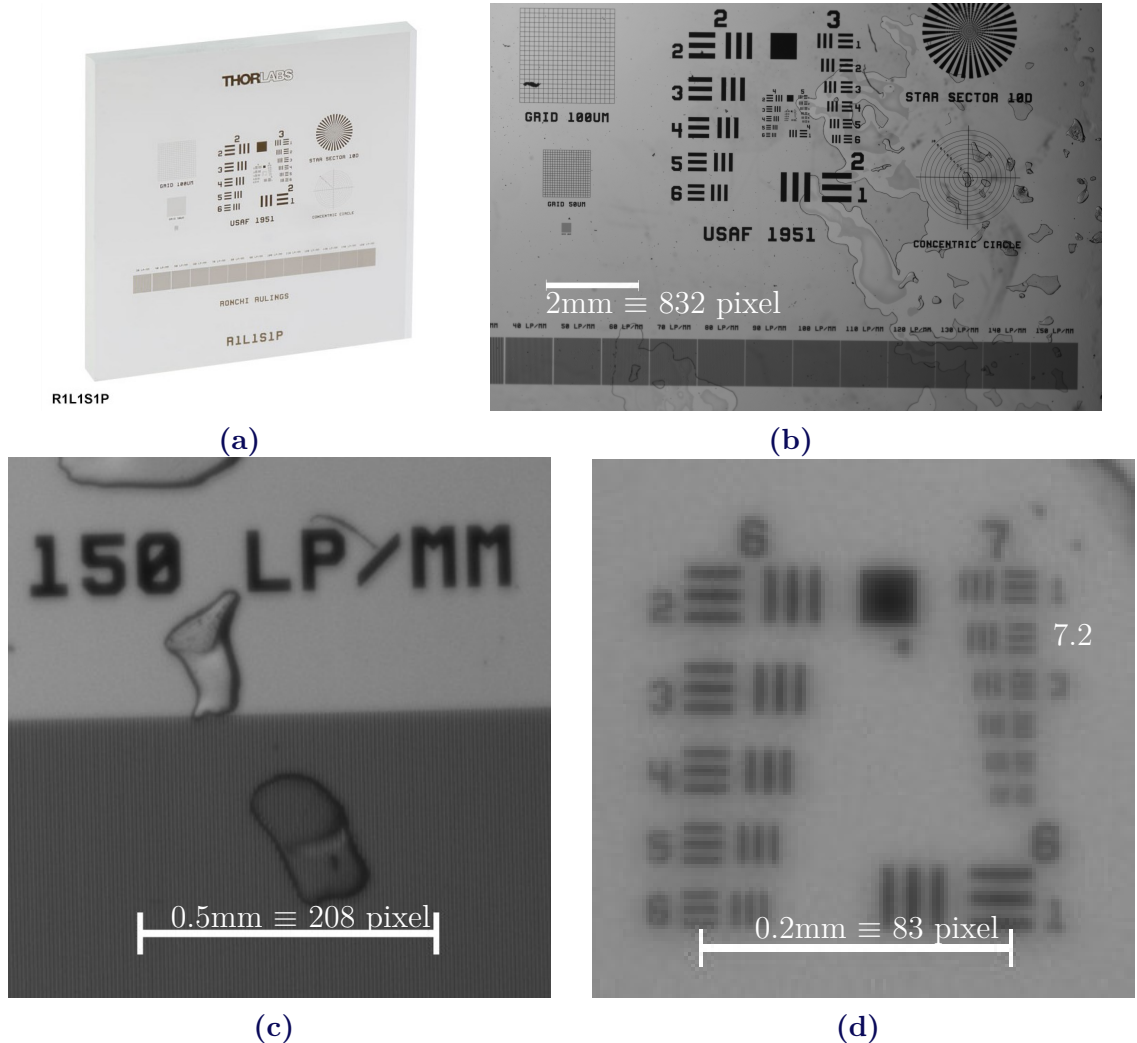


Figure 4.3: a) USAF resolution test target in full size, adapted from [19]. b), c) and d) are zoomed in versions of it with different digital enlargements. The maximum resolution of the USAF target can be found in Figure d). The position marked with white letters in group 7 and element 2 corresponds to a resolution of 143.7 lp/mm.

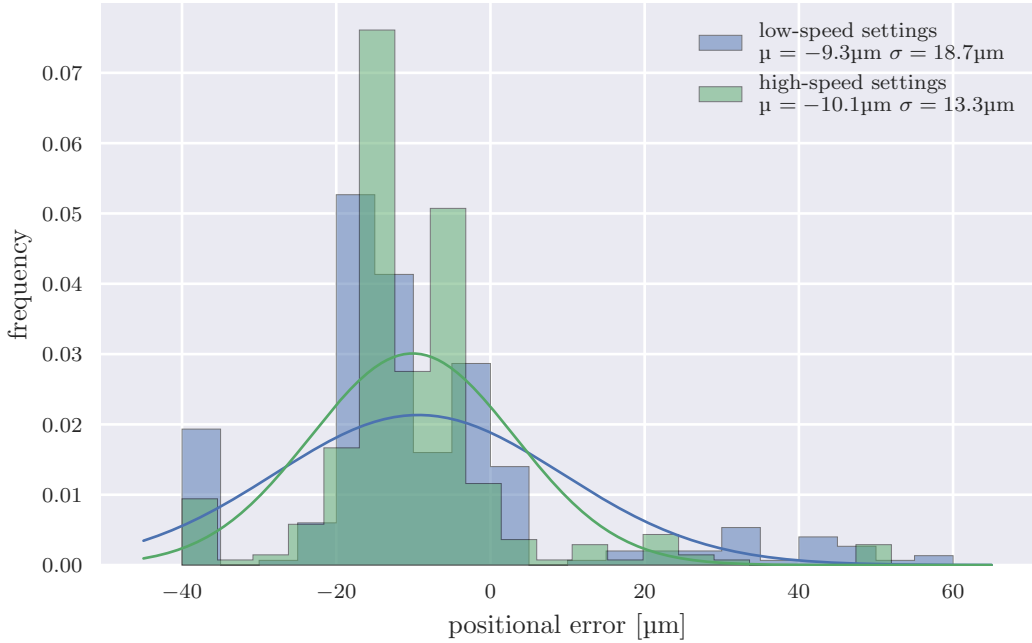


Figure 4.4: Positioning Performance: The corrections during repositioning were analyzed to describe the position accuracy. This repositioning was repeated done 150 times for different speeds after running through 96 positions.

4.2 Actuators: precision and performance

4.2.1 Positioning performance

The accuracy describes the difference between the actual and the expected position of a mechanical system. For this measurement, an experiment run generated the data: 96 positions were set before the final position was checked. One of these runs takes approximately four minutes. 200 runs were analyzed for this measurement. In [Figure 4.4 Positioning performance](#) a histogram of the position errors on all four axes is shown. The test was carried out with different speed settings, whereby both the maximum speed and the acceleration were varied. The speed settings do not indicate an influence on the positioning accuracy. The possible maximum errors of $\pm 60 \mu\text{m}$ are negligible in the current constellation of macroscopy. The mean (μ) and the standard deviation (σ) are shown in the legend of the figure. Another possible interpretation from the field of motor accuracy concludes the μ represents repetition accuracy and σ represents accuracy.

4.2.2 Theoretical resolution

The resolution repeats the smallest possible movement that can be achieved by the system. The theoretical resolution is the length of one micro step from the stepper motor. With 110 mm travel per motor revolution, 200 steps per motor revolution and 128 micro-steps per step, this corresponds to $4.296875 \mu\text{m}$. The actual accuracy can be estimated with mean (μ) and the standard deviation of the repositioning (see [Figure 4.4 Positioning performance](#)).

	X-Direction				Y-Direction				Run-time s	Accuracy μm
	Max Speed step/s	Speed mm/s	Acceleration step/s ²	mm/s ²	Max Speed step/s	Speed mm/s	Acceleration step/s ²	mm/s ²		
Slow	400	220	50	27.5	400	220	50	27.5	401	84
Medium	900	495	3000	1650	600	330	500	275	117	80
Fast	4000	2200	3000	1650	2000	1100	1000	550	110	70

Table 4.1: Pre-installed parameters for the basic kinematics of the robot. In addition to the maximum speed and acceleration values for each axis, the right two columns contain the resulting experiment values. The runtime results after 96 positions, including one second per position to take pictures and a recalibration of the position. The repositioning accuracy in the last column is calculated as the $3 * (\mu + \sigma)$ from Figure 4.4 Positioning performance

4.2.3 Speed

For each of the four axes, the maximum speed and acceleration are defined in the Robo-class in Matlab (see [Figure 3.17 Software component diagram](#)). Both can be varied during operation. The usage of the stepper motor driver is accompanied with the significant advantage of a smooth acceleration and slowing down mechanism. Consequential, that even heavy cameras or light sources can be moved. Nevertheless, the robot would be damage, if the speed parameters that are too high. Three speeds settings are programmed and tested for full operation with 96 positions. These parameters are shown in [Table 4.1 Pre-installed kinematic parameters](#).

CHAPTER 5

Optimization swarming protocol

This protocol is optimized to analyse Koo's *B. subtilis* library's swarming behaviour. The aim is to describe the 4400 mutants with physical and visible swarming properties. The optimization is based on the *B. subtilis* wild type. The more precisely this behavior can be described, the more clearly the differences to the mutants are becoming visible.

The size of the Petri dish influences the maximum measuring time, which continues until a swarm of bacteria has reached the edge of the dish. A longer measurement time leads to more precise and deeper insights into the morphological development and the change in the rate of propagation over time. According to priority work from H. Jeckel [4], an exponential front expansion is expected. The disadvantage of large Petri dishes is induced by a more cumbersome handling. The requirement of a high throughput setup is calling for an observation of at least 48 bacteria during a run, but with a consequential size at a range which is easily to handle. To screen 96 bacteria in parallel is useful since this is the standard number in the 96-well plate in which the 3968 mutant library is available. With 96 mutants per run, 42 individual experiments are approximately 3 hours for preparation and 6 hours for measurement. The experiments were carried out with three different sizes of 90, 55 and 35 mm to find the optimal Petri dish size. [Figure 5.1 Petri dish variation](#) shows the reproducibility of growth curves of *B. subtilis* wild type in different Petri dish sizes. The fit parameters vary the least with 55 mm Petri dishes.

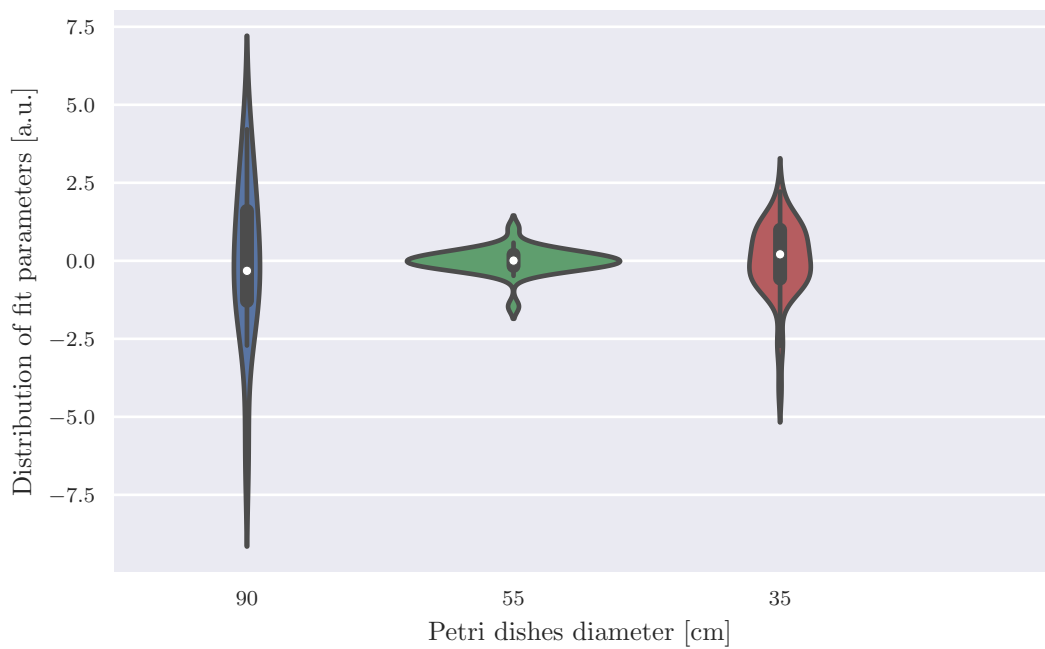


Figure 5.1: After the front of the swarm was detected at every point in time. An exponential function was fitted on the swarm diameter. The distribution of the fit parameters shows how strongly the parameters vary in different experiments. The deviation from the mean is shown. Therefore, a peak distribution at 0 would be ideal.

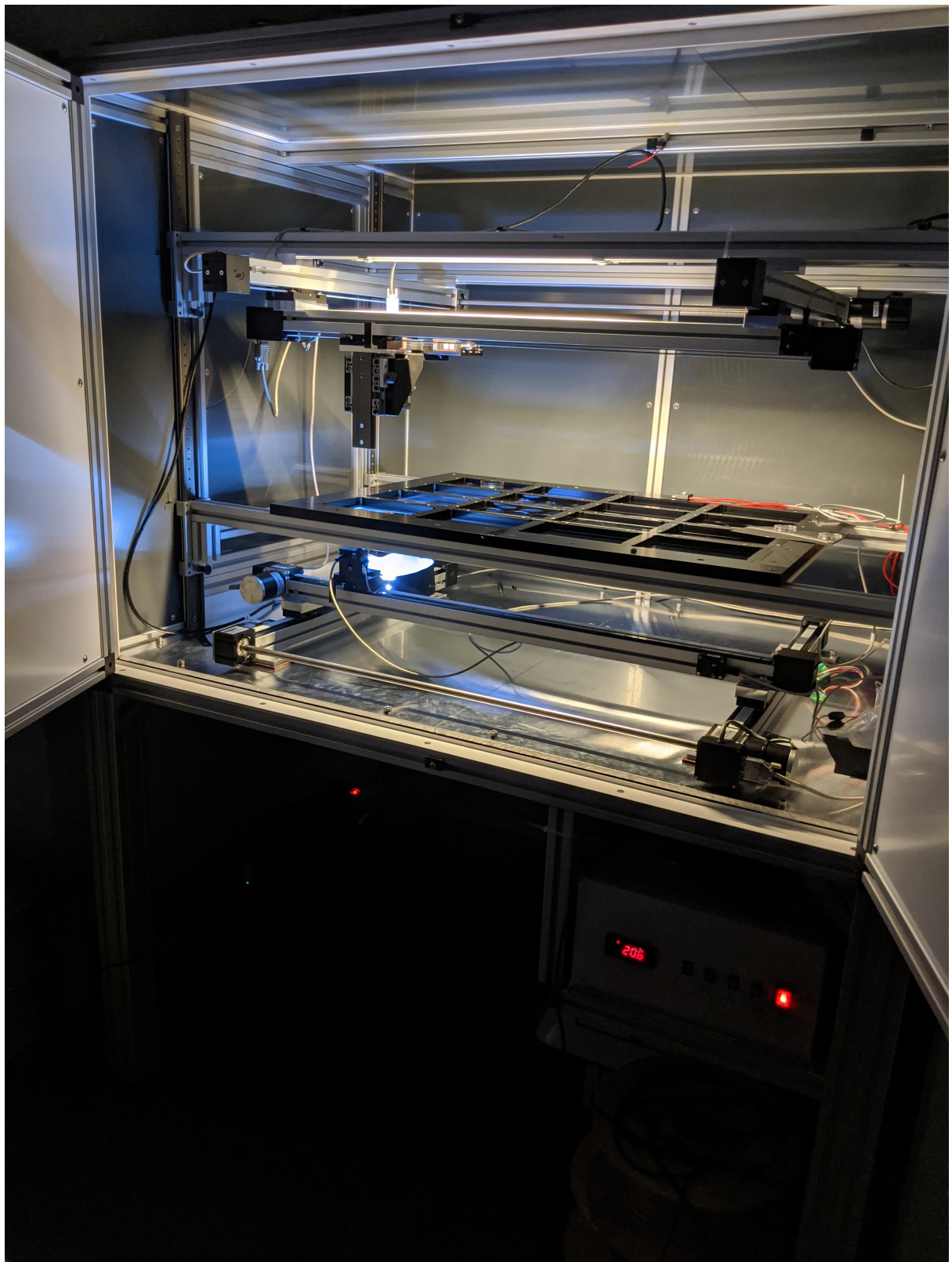
CHAPTER 6

Conclusions

The aim scope of this project was to the preparation and implementation towards the screening of an *B. subtilis* KO library's swarm development. It was decided to use a High-Throughput Screening (HTS) to handle the large number of mutants in this library. The large number was further transformed into a swarming background with total DNA isolation. The implementation and first measurement are described within this work. Here, the measurements had to be carried out using a dark field imaging to ensure the visibility of the monolayer of bacteria. The optical imaging was added by two lightning setups, a heatable environment and an automatized sample preparation. Furthermore, the software for controlling and readout was written to make the robot easy to use. The camera and light source can be positioned with an accuracy of 70 µm. The optical imaging capability with a pixel size of up to 3.33 µm extends the possible uses of the robot.

The first results were obtained with the scope to study the swarming behavior of *B. subtilis* and to confirm an exponential growth rate. This topic connects to the previous study by Hannah Jeckel, describing the dynamics of a swarming colony on a microscopic scale. The robot ensured a measurement of 96 target samples in 2 min. Hence, various genetic phenotypes and studied by reproducible experimental conditions.

In the future, fluorescence applications will be further developed and thus show additional insights into gene expression on macroscopic scales.



List of Figures

2.1	Bacterial motility	4
2.2	Swarming colonies	5
2.3	Schematic Dark Field Illumination	6
3.1	96-Microplate replicator	10
3.2	Proof of concept model	13
3.3	first design	15
3.4	Ring lights homogeneity	17
3.5	<i>B. subtilis</i> after 4h	18
3.6	Lighting test	19
3.7	Multi Swarming result	19
3.8	Optical setup	21
3.9	Vibirio cholera microscopic	22
3.10	Heating test	24
3.11	Surface temperatures	25
3.12	Plate holder	26
3.13	Electronics box insight	28
3.14	Circuit diagram	29
3.15	Temperature controller front panel	30
3.16	GUI layout	31
3.17	Software component diagram	32
4.1	Final design	34
4.2	Emission distribution	34
4.3	Practical image resolution test	36
4.4	Positioning performance	37
5.1	Petri dish variation	40

Bibliography

- [1] D. B. Kearns, “A field guide to bacterial swarming motility,” *Nature reviews. Microbiology*, Sep 2010.
- [2] X. Chen, X. Dong, A. Be’er, H. L. Swinney, and H. P. Zhang, “Scale-invariant correlations in dynamic bacterial clusters,” *Physical Review Letters*, Apr 2012.
- [3] H. P. Zhang, A. Be’er, E.-L. Florin, and H. L. Swinney, “Collective motion and density fluctuations in bacterial colonies,” *Proceedings of the National Academy of Sciences of the United States of America*, Aug 2010.
- [4] H. Jeckel, E. Jelli, R. Hartmann, P. K. Singh, R. Mok, J. F. Totz, L. Vidakovic, B. Eckhardt, J. Dunkel, and K. Drescher, “Learning the space-time phase diagram of bacterial swarm expansion,” *Proceedings of the National Academy of Sciences*, vol. 116, no. 5, pp. 1489–1494, 2019.
- [5] M.-H. Beydon, A. Fournier, L. Drugeault, and J. Becquart, “Microbiological high throughput screening: An opportunity for the lead discovery process,” *SAGE Journals*, Feb 2000.
- [6] J. Henrichsen, “Bacterial surface translocation: a survey and a classification,” *Bacteriological reviews*, Dec 1972.
- [7] J. E. Patrick and D. B. Kearns, “Laboratory strains of bacillus subtilis do not exhibit swarming motility,” *Journal of bacteriology*, Nov 2009.
- [8] H. E. Jones and R. W. A. Park, “The influence of medium composition on the growth and swarming of proteus,” *Microbiology*, Jun 1967.
- [9] R. M. Harshey, “Bacterial motility on a surface: Many ways to a common goal,” *Annual Review of Microbiology*, vol. 57, no. 1, pp. 249–273, 2003. PMID: 14527279.
- [10] M. Silverman and M. Simon, “Flagellar rotation and the mechanism of bacterial motility,” *Nature News*, May 1974.

- [11] F. F. V. Chevance and K. T. Hughes, “Coordinating assembly of a bacterial macromolecular machine,” *Nature News*, Jun 2008.
- [12] N. Verstraeten, K. Braeken, B. Debkumari, M. Fauvert, J. Fransaer, J. Vermant, and J. Michiels, “Living on a surface: swarming and biofilm formation,” *Trends in Microbiology*, Sep 2008.
- [13] M. Bass and O. S. of America, *Handbook of optics*. No. Bd. 1-2 in Handbook of Optics, McGraw-Hill, 2001.
- [14] B.-M. Koo, G. Kritikos, J. D. Farelli, H. Todor, K. Tong, H. Kimsey, I. Wapinski, M. Galardini, A. Cabal, J. M. Peters, and et al., “Construction and analysis of two genome-scale deletion libraries for bacillus subtilis,” *Cell systems*, Mar 2017.
- [15] R. S. Shapiro and L. E. Cowen, “Thermal control of microbial development and virulence: Molecular mechanisms of microbial temperature sensing,” *mBio*, vol. 3, no. 5, 2012.
- [16] “Din en iso 13732-1:2008-12: Ergonomie der thermischen umgebung.” <https://www.beuth.de/de/norm/din-en-iso-13732-1/111624965>, Last accessed on 2020-02-03.
- [17] RS Online, “Instruction manual for eng esm-3721 heating controller,” 2014. <https://docs.rs-online.com/f067/0900766b815852a4.pdf>, Last accessed on 2020-01-03.
- [18] Sony Corporation, “Flyer for imx183,” 2019. https://www.sony-semicon.co.jp/products/common/pdf/IMX183CLK-J_CQJ-J_Flyer.pdf, Last accessed on 2019-12-31.
- [19] Thorlabs, Inc., “Combined resolution and distortion test targets.” https://www.thorlabs.de/newgroupage9.cfm?objectgroup_id=4338, Last accessed on 2020-01-03.

Acknowledgement



I thank Prof. Dr. Knut Drescher for the provision of the interesting and productive topic and the correction of this thesis. I also thank him for the guidance and hints he provided to ensure steady progress and thought out experiments.

I also thank Prof. Dr. Victor Sourjik for being available as the second reviewer of this thesis.

Furthermore, I thank Horst Henseling for being a excellent Precision Engineer. With your ideas and the high-precision implementation, you have taken this project very far.

My thanks go to all members of AG Drescher, for providing a productive and fun work environment.

I also thank all my friends for the support, especially Meli and Sebastian. You brought the ship to the safe harbor.

Finally, I thank my family for funding my studies and for the overall support.

Erklärung

Hiermit erkläre ich, dass ich meine Masterarbeit mit dem Thema:

**Screening for physical and biological determinants
of bacterial swarm development**

selbstständig verfasst sowie alle wesentlichen Quellen und Hilfsmittel angegeben habe.

Name, Vorname: Brieden, Sven

Ort, Datum: Marburg, 07.02.2020

Unterschrift: